J. Fluid Mech. (2010), *vol.* 654, *pp.* 417–451.
doi:10.1017/S0022112010000650

On the diffusion of circular domains on a spherical vesicle

S. ALIASKARISOHI[1], P. TIERNO[2], P. DHAR[3], Z. KHATTARI[4], M. BLASZCZYNSKI[1] AND TH. M. FISCHER[1]†

[1]Institut für Experimentalphysik, Universität Bayreuth, 95440 Bayreuth, Germany

[2]Departament de Química Física, Universitat de Barcelona, Marti i Franqes 1, 08028 Barcelona, Spain

[3]Department of Chemical Engineering, University of California Santa Barbara, Santa Barbara, CA 93106, USA

[4]Department of Physics, Hashemite University, 13115 Zarqa, Jordan

(Received 17 August 2009; revised 2 February 2010; accepted 2 February 2010; first published online 11 May 2010)

Tracking the motion of lipid domains on a vesicle is a rheological technique allowing the measurement of surface shear viscosities of vesicular lipid phases. The ratio of surface to bulk viscosity defines a viscous length scale. Hydrodynamic interactions split the motion of the domains into different modes of diffusion. The measurability of surface shear viscosities from any mode of diffusion is limited to viscous length scales between the radius of the domains and the radius of the vesicle. The measurability of the surface shear viscosity results from the sensitivity of the diffusion to surface shear viscosities and from sufficient spatial resolution to resolve the diffusive motion. Switching between the various modes of diffusion is a trade between sensitivity gained and resolution lost by the hydrodynamic interactions leaving the measurability unchanged. Measurability drops with the number of domains making single-domain rheology the best technique to measure surface shear viscosities. Ultimately confinement of the domains to small vesicles renders measurements of surface rheological properties with domain-tracking rheology impossible. Experiments on domains in vesicles of a mixture of dioleoylphosphatidylcholine (DOPC), dipalmytoylphosphatidylcholin (DPPC) and cholesterol (Chol) exhibit diffusion that is entirely controlled by dissipation into the water. The diffusion is suppressed compared to the diffusion of isolated domains in a flat membrane due to confinement to the curved vesicle and by hydrodynamic interactions between the domains. Effects of surface shear viscosity can be neglected.

1. Introduction

Diffusion is one of the basic passive means of irreversible transport used in the cell as well as in membranes. In comparison to active forms of transport, diffusion does not cost any energy. Without interaction between components, diffusion will ultimately lead to thermal equilibrium with a complete mixture of the components. Along those lines (Singer & Nicholson 1972) originally modelled biological membranes as an ideal two-dimensional mixture of lipids and proteins that was initially described by the fluid mosaic model. Later it has been realized that despite the tendency to mix, lipids

† Email address for correspondence: thomas.fischer@uni-bayreuth.de

interact. The interaction causes demixing into membrane domains ('rafts') (Simons & Ikonen 1997; Brown & London 1998; Mukherjee & Maxfield 2000; Gaus *et al.* 2003; Engelman 2005) consisting of a phase rich in cholesterol, certain types of lipids and proteins, and a complementary phase containing the complementary composition of the lipids. The mesoscopic structure which in part is caused by the enthalpy of mixing of the components has triggered research towards understanding the interactions of two-dimensional model mixtures. Experiments on monolayer mixtures Radhakrishnan & McConnell (1999) and later on giant unilamellar vesicles (Korlach *et al.* 1999; Bagatolli & Gratton 2000; Veatch & Keller 2002) has shown that especially the mixtures of phospholipids and cholesterol can be understood as thermodynamic equilibrium mixtures. Miscibility diagrams determined from the experiments could be described with theories minimizing the Gibb's free energy of the reactive mixture. The long term stability of domains of different composition allows treating such domains as entities with their own transport properties. Cicuta, Keller & Veatch (2007) showed that such domains undergo diffusive motion. The dynamics of the domains are governed by the viscous properties of the participating two- and three-dimensional phases (Saffmann & Delbrück 1975; Hughes, Pailthorpe & White 1981) as well as by their geometrical arrangement (Dimova *et al.* 1999*a*; Dimova, Dietrich & Pouligny 1999*b*; Danov, Dimova & Pouligny 2000; Fischer, Dhar & Heinig 2006). The work of Saffmann & Delbrück (1975) originally derived for small solid and disk shaped inclusions of proteins into a flat and highly viscous membrane has been subject of both experimental tests (Peters & Cherry 1982; Klingler & McConnell 1993; Daniels & Turner 2002; Naji, Levine& Pincus 2007; Sickert, Rondelez & Stone 2007) and theoretical generalizations (Prasad, Koehler & Weeks 2006; Petrov & Schwille 2008). The knowledge of rheological properties of complex membranes or monolayers is an important experimental issue and one would like to understand how the addition of cholesterol (Veatch & Keller 2003; Beattie *et al.* 2005; Veatch, Gawrisch & Keller 2006), synthetic fluorinated compounds (Riess 2002) and the presence of electrostatic interactions (Heinig *et al.* 2002; Khattari *et al.* 2002; Fischer & Lösche 2004) alter the membrane or monolayer viscous behaviour. The purpose of this work is to generalize the theory of Saffmann & Delbrück (1975) for circular domains diffusing on a vesicle. One of the important findings of Saffmann & Delbrück (1975) was that the ratio of the membrane to the bulk viscosity defines a viscous length scale. Therefore, the motion of objects moving in a membrane depends on how the size of these objects compares to the viscous length scale. Diffusion of domains on a vesicle differs from the calculations of Saffmann & Delbrück (1975) in four important aspects. Firstly, the surface viscosity of the membrane embedding the domain in general can be either low or high. A theory taking into account the full range of possible surface shear viscosities of the embedding membrane has been first derived by Hughes *et al.* (1981). Secondly, since the domains on the vesicle, like the embedding membrane, are in general liquid not solid, the domain surface shear viscosity plays an important role. De Koker (1996) was the first to derive a hydrodynamic equation for a liquid domain diffusing in a flat membrane of the same surface shear viscosity. Thirdly, the vesicle consists of a curved membrane and therefore has a finite size. As a consequence of its finite size, the vesicle will perform rotational diffusion while the domain is diffusing on its surface. The apparent motion of a domain observed on the vesicle surface with microscopic techniques is hence a superposition of both kinds of diffusive motions. When being interested in extracting rheological properties of the vesicle membrane from the domain diffusion the rotational diffusion of the vesicle in the water is disturbing. One might eliminate solid rotations of the vesicle

by tracking the relative motion between several domains on the same vesicle, which is independent of the rotation of the vesicle as a whole. However, such two-domain rheology introduces the separation of the domains as a new length scale to the problem, and our mathematical results presented in this manuscript results show cross-over from uncorrelated to strongly correlated relative motion when this new length scale becomes smaller than the viscous length scale. As a fourth complication, the hydrodynamic correlations between the domains are different for different modes of motion. Here we derive the hydrodynamic equations that govern such diffusion for a single-liquid bilayer domain diffusing on a vesicle and for the combined and the relative diffusion of two liquid bilayer domains. For the single-domain diffusion we will show that there is a cross-over from surface viscous dominated diffusion to a solid rotational diffusion of the entire vesicle when the size of the vesicle is smaller than viscous length scale. For the two-domain rheology the same cross-over manifests itself by a change from uncorrelated diffusion of the two domains towards a correlated diffusion. This behaviour also occurs for two domains in a flat membrane and the theory of two particle microrheology (Prasad *et al.* 2006) differs from single-domain rheology for the case of a flat membrane. Our results provide a theoretical tool to analyse recent (Cicuta *et al.* 2007) measurements of surface shear viscosity of domains diffusing on curved membranes. We additionally apply the theory to new measurements of the same system. The paper is organized as follows. In § 2 we describe some general aspects of measuring diffusion on curved vesicles. In § 3 we describe how to perform a single-domain rheology experiment. Section 4 describes the decomposition of the motion of two domains into four normal modes of motion and the experimental extraction of the dimensionless diffusion coefficient. Section 5 outlines the theory for the computation of the dimensionless diffusion coefficient as a function of the geometrical details and as a function of the various rheological properties of the participating fluids. Sections 6 and 7 present experimental and numerical results for the single-domain and two-domain diffusion coefficients, respectively. We compared both techniques and comment on their limitations. Section 8 discusses our model in the context of our and others experimental findings and § 9 gives a summary.

2. Experimental

We consider a set of $i = 1 \ldots n$ diffusing domains as liquid circular segments of radii a_i on a spherical vesicle of radius R (figure 1). A fluorescence microscope image of such a vesicle is depicted in figure 1. It shows a vesicle of radius $R = 12\,\mu\text{m}$ of a mixture of dioleoylphosphatidylcholine (DOPC), dipalmytoylphosphatidylcholin (DPPC) and cholesterol (Chol) of composition (DOPC/DPPC/Chol = 16/64/20) at a temperature of $T = 23^{\circ}\text{C}$. The mixture decomposes into an L_α phase visible as bright domains of average size $a = 1$–$3\,\mu\text{m}$ and into a L_0 and a S_0 phase (Veatch & Keller 2003) that both appear dark and are not distinguishable in the fluorescence image. DOPC, DPPC and Cholestrol were purchased from Avanti Polar Lipids. Mixtures were fluorescently labelled with 1 %–3 % of 1,2-dihexadecanoyl-sn-glycero-3-phosphoethanolamine, triethylammonium salt (Texas Red DHPE) which was purchased from Molecular Probes (Eugene, Oregon USA). Giant unilamellar vesicles were prepared using the electroformation method as described by Angelova *et al.* (1992) and Veatch & Keller (2002). Lipids were dissolved in chloroform/methanol 9:1 at a concentration of 2 mg ml^{-1}. A drop of 10 µl was deposited onto the conductive side of an indium tin oxide (ITO) coated glass slide and dried using a nitrogen stream.

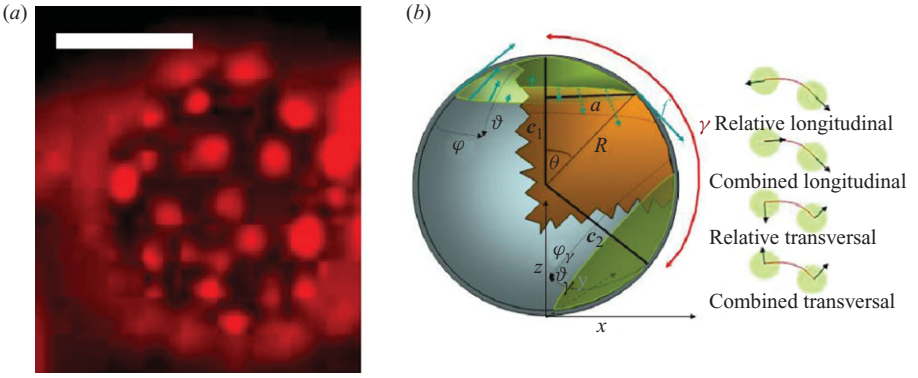

FIGURE 1. (*a*) Fluorescence microscopy image of a vesicle of radius $R = 12\,\mu\text{m}$, consisting of a mixture of DOPC/DPPC/Chol of composition 16/64/20 that decomposes into an L_α phase (bright domains), and into a L_0 and a S_0 phase that cannot be distinguished (continuous dark region). The scale bar corresponds to a distance of 10 μm. The scope of this paper is to describe the origin of diffusion of the domains in the vesicle. (*b*) Scheme of two lipid domains (green) of radius a centred at position $\boldsymbol{c}_1$ and $\boldsymbol{c}_2$ and diffusing on a vesicle of radius R. The domains have a conical domain angle of θ and γ is the separation angle. The force profile normal to the edges (cyan arrows) of the domains arising from thermal fluctuations or external forcing causes the domains diffusion. Shown are also the coordinates (ϑ, φ) defined with respect to the z-axis and the second coordinate system $(\vartheta_\gamma, \varphi_\gamma)$ defined with respect to the $\boldsymbol{c}_2$-axis. The four possible modes of diffusion of the domains are depicted on the right. The red line is the interconnecting geodesic between the domains and the black arrows indicate the velocities of the domains. Longitudinal modes correspond to motion in direction of the geodesic. Transversal modes correspond to motion perpendicular to the geodesic. Combined motion is into the same direction while relative motion is into antiparallel directions. The terms 'parallel' and 'direction' are used in the sense of the curved metric on the surface of the vesicle not in the sense of three-dimensional Euclidian metric.

The sample was then put in vacuum for 1–3 h at 60°C. A silicone spacer was deposited around the dried lipids and 0.2 M sucrose solution in pure water (Millipore milli-Q water) was added. By sealing the slide with another ITO Plate a capacitor was formed and an AC field was applied for 2 h and 10 min at 60 ± 3°C. For applying the AC field two different schemes were used and both of them gave us nice vesicles. In the first scheme, the voltage was increased from 0.2 to 2 V in 10 min and the swelling time under the AC field was 100 min. Finally, the voltage is decreased from 2 to 0.2 V at a frequency of 1 Hz within 20 min to lay down the vesicles. In the second scheme, the voltage was increased from 0.2 to 2 V at 10 Hz within 10 min then the frequency was decreased to 1 Hz and kept there for 100 min. The lay down frequency was 0.5 Hz instead of 1 Hz. The grown vesicles were stored at room temperature (24°C) in the dark until use. The best time for observation was between 1 and 12 h after electroformation. Vesicles were sucked out from the chambers and put on the microscope glass slide, 20 μl glucose solution was added. A coverslip (0.17 mm) was used with tape spacers (0.1 mm) to observe the samples and a fluorescence microscope (LEICA DM 4000B) with a $\times 63$ air objective was used for visualization. The working distance of the objective was 0.31 mm which allowed to observe vesicles floating at a distance of 140 μm from the cover slide. In order to avoid hydrodynamic interactions with the upper cover slide and the lower glass slide we always worked with vesicles spaced at least 2 diameters from both slides. The vesicles were investigated at room temperature 23 ± 1°C. Frames were captured with a camera (BASLER A311fc) having 640×480 pixels at a resolution of 6 pixels μm^{-1} and a frame rate of

27 frames s^{-1}. The optical resolution was of the order of a micron. Typical recording times of one particular vesicle were of the order of 15 s. The time limitation for the recording was mainly caused by bleaching of the fluorecence dye and did not reach the physical limit set by the rotational and translational diffusion of the entire vesicle.

The central position of each domain on the vesicle as a function of time can be characterized by the vector $\boldsymbol{c}_i = R(\sin\vartheta_i\cos\varphi_i, \sin\vartheta_i\sin\varphi_i, \cos\vartheta_i)$, where $\vartheta_i(t)$ and $\varphi_i(t)$ are the polar and azimuth angle. In a domain diffusion experiment the raw data are the time dependent vectors $\boldsymbol{c}_i(t)$ pointing to the centres of the domains. The vertical position z of the domain can be constructed from the lateral position assuming a spherical shape of the vesicle.

A change in position of a domain on a vesicle is not necessarily due to translational diffusion through the membrane. This can be easily seen by considering a vesicle with very high viscosity of the bilayer. In a flat membrane an infinite membrane viscosity would simply impede any translational diffusion. A vesicle however can perform rotational diffusion in the same way a solid sphere reorients in a liquid. In the generic case both types of motion are coupled. A decoupling of both types of motion can be either performed experimentally by measuring the motion of a domain 'relative' to some reference domains. We will discuss the simplest form of measuring such 'relative' motion in § 4 dedicated to two-domain rheology. The other possibility is to measure the absolute motion of a domain and derive a theoretical expression for the total diffusion of the domain. In § 3 we follow the second approach.

There are two ways to look at the diffusion of a domain on the vesicle. One is to watch the domain from three-dimensional space, the other is to consider the domain moving in a two-dimensional curved space. If we consider the first point of view, we would say that the domain is confined to the vesicle surface and the domain moves in an erratic way on the surface around the centre of the vesicle. Thus the motion of the domain is a rotational diffusion of the domain around the vesicle centre. According to the second point of view the diffusion of the domain is an erratic 'translational' motion through a curved membrane. Both points of view have their advantages. The advantage of the three-dimensional approach is that the three-dimensional space is Euclidian, while the membrane surface is non-Euclidian. We will distinguish motions described by the 'non-Euclidian' point of view from the Euclidian point of view by marking it in quotes throughout the text. Euclidian rotational motion of the domain is mathematically easier to describe than non Euclidian 'translational' motion. Let us consider the Euclidian point of view: an infinitesimal change in domain position during the time $\mathrm{d}t$ occurs due to an infinitesimal rotation $\mathrm{d}\boldsymbol{c}_i = \boldsymbol{\omega}_i \times \boldsymbol{c}_i \, \mathrm{d}t$ of the position, where $\boldsymbol{\omega}_i$ denotes the momentary angular frequency of rotation of the ith domain around the vesicle centre. Hence the diffusion of the domain is characterized by the rotational diffusion of the orientation of the vector $\boldsymbol{c}_i$ on the vesicle surface in the same sense as a director of a nematic liquid crystal performs rotational diffusion. The three-dimensional rotational diffusion should not be confused with the two-dimensional 'rotational' diffusion of the domain in the membrane which corresponds to 'rotations' of a domain around the domain centre not to rotations of a domain around the vesicle centre. In this work the term rotational diffusion will always correspond to the rotation of the domain around the vesicle centre.

In general, the diffusion of the domains will depend on their geometrical arrangement on the vesicle, described by the domain sizes and their polar and azimuthal angles. Two arrangements of the domains will have the same diffusion constants if the two arrangements can be mapped on top of each other by a solid rotation. Instead of using individual coordinates of the domains, we might use three

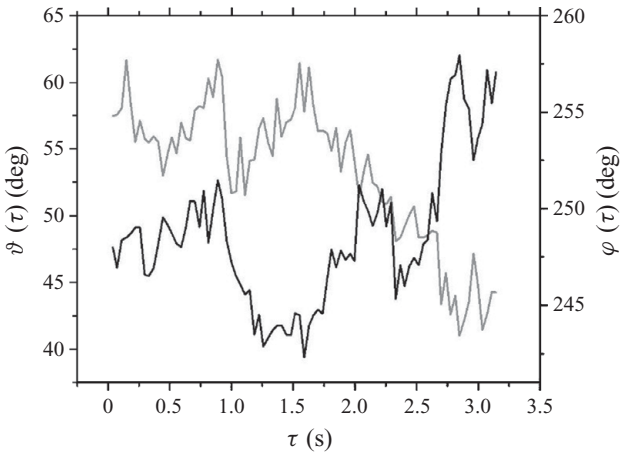

FIGURE 2. Time evolution of the polar and azimuthal angle of a domain of size $a = 0.7\,\mu\text{m}$ in a vesicle of size $R = 7.4\,\mu\text{m}$ of composition (DOPC/DPPC/Chol = 40/40/20) at temperature $T = 23^{\circ}\text{C}$.

Euler angles to describe the solid rotation of all domains on the vesicle and a set $\mathscr{C}$ of conformational coordinates describing the relative conformation of the domains. Using these conformational coordinates we may define the diffusion constant $D_{ij}(\mathscr{C})$ of a specific conformation via the correlation function of the angular velocity fluctuations of the domains following the general theory of Kubo (1957):

$$D_{ij}(\mathscr{C}) = \int_0^\infty \mathrm{d}\tau \langle \boldsymbol{\omega}_i(t)\boldsymbol{\omega}_j(t+\tau)\rangle_{\mathscr{C}}, \tag{2.1}$$

where

$$\langle X\rangle_{\mathscr{C}} = \int \mathrm{d}\mathscr{C}' \int \mathrm{d}t\, X(\mathscr{C}', t)\delta(\mathscr{C} - \mathscr{C}') \tag{2.2}$$

denotes the ensemble and time average over all arrangements having the conformation $\mathscr{C}$. If there are more than one domain, the diffusion constant becomes a symmetric tensor and a diagonalization yields the eigenvalues $D_\lambda(\mathscr{C})$ of the different normal modes of diffusion for the conformation $\mathscr{C}$.

3. One-domain rheology: experiment

For the case of one single domain diffusing in a vesicle the only conformational variable is the conserved size $a = R\cos\theta$ of the domain. Here θ denotes the conical opening angle of the domain on the vesicle (figure 1). Since all conformational coordinates are invariants of the diffusive motion, there exists a description of rotational diffusion that is analogous to the description of diffusion in flat systems in terms of a mean square displacement. Using spherical coordinates the position of the domain can be described by the polar and azimuthal angles (ϑ, φ) of the centre of the domain. Figure 2 shows the time evolution of the domain position as a function of time for a domain of size $a = 0.7\,\mu\text{m}$ in a vesicle of size $R = 7.5\,\mu\text{m}$ of composition (DOPC/DPPC/Chol = 40/40/20) at temperature $T = 23^{\circ}\text{C}$. The diffusion of the domain results in fluctuations of the polar and azimuthal angles.

The role of displacement is taken by the angular separation between the domain at different times. The angular separation between the position on the sphere at time t_i

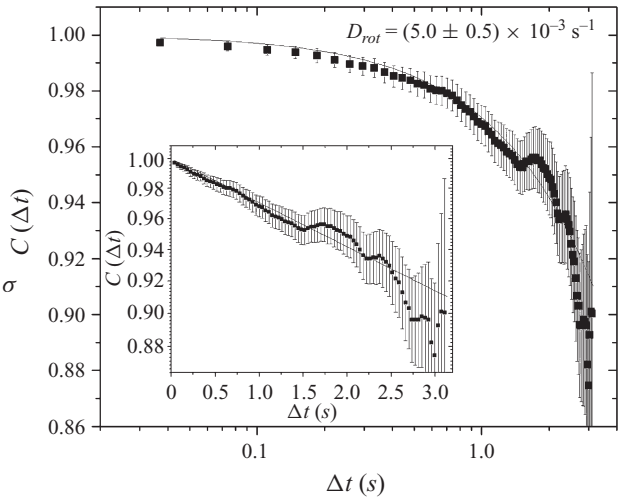

FIGURE 3. Plot of the experimental rotational correlation function $C(\Delta t)$ as computed from the domain trajectory of figure 2 via (3.1) (symbols) together with a fit to a random walk diffusion according to (3.2) (line graph). The inset shows the same data on a linear time scale. The exponential decay is indistinguishable from a linear decay since the correlation time was much shorter than the rotational diffusion constant.

and time t_j is then given by the angle $\cos(\gamma(t_i, t_j)) = \mathbf{c}(t_i) \cdot \boldsymbol{c}(t_j) = \cos\vartheta(t_i)\cos\vartheta(t_j) + \sin\vartheta(t_i)\sin\vartheta(t_j)\cos(\varphi(t_i) - \varphi(t_j))$. We define the angular correlation function following Berne & Precora (2000):

$$C(\Delta t) = \frac{\sum_{i,j} \delta_{\Delta t, t_j - t_i} P_2(\cos(\gamma(t_i, t_j)))}{\sum_{i,j} \delta_{\Delta t, t_j - t_i}}, \tag{3.1}$$

where $\delta_{\Delta t, t_j - t_i}$ denotes the Kronecker delta and Δt is the time separation between t_i and t_j and the sum is taken over all pairs of data taken at different times having the same time separation. $P_2(\cos\gamma) = 3/2\cos^2\gamma - 1/2$ is the Legendre polynomial of degree 2. The definition of the angular correlation function in (3.1) is the same as used for the director orientation in liquid crystals (Berne & Precora 2000). For a random walk of the domain on a spherical surface, the rotational correlation function exponentially decreases with the time lag Δt as (Berne & Precora 2000)

$$C(\Delta t) = \mathrm{e}^{-6 D_{rot} \Delta t}, \tag{3.2}$$

where D_{rot} denotes the rotational diffusion constant of the domain. Hence a fit of the angular correlation function equations (3.1) to (3.2) will yield the rotational diffusion constant.

Figure 3 shows the angular correlation function $C(\Delta t)$ as computed from the domain trajectory of figure 2 via (3.1) together with a fit to a random walk diffusion according to (3.2). The fit describes the data well for smaller correlation times. At large times the experimental data starts deviating since there is insufficient statistics. Such decrease in statistics with the correlation time is inherent to all experimental correlation functions. The fit corresponds to a rotational diffusion constant of $D_{rot} = 5.0 \times 10^{-3}\,\mathrm{s}^{-1}$.

On short time scales the probability to diffuse away far from the original position is low such that the domain will not sense the confinement imposed by the curved surface of the vesicle. Hence in the limit $\Delta t \to 0$ also the angle γ vanishes ($\gamma \to 0$)

and we might expand (3.1) and (3.2) to obtain the connection of the three-dimensional rotation diffusion constant with the apparent two-dimensional 'translational' diffusion of the domain. We find

$$\lim_{\Delta t\to 0} P_2(\cos\gamma) = 3/2\cos^2\gamma - 1/2 \to 1 - 3/2\gamma^2 \tag{3.3}$$

and

$$\lim_{\Delta t\to 0} \mathrm{e}^{-6D_{rot}\Delta t} \to 1 - 6D_{rot}\Delta t. \tag{3.4}$$

From (3.3) and (3.4) we conclude that in the tangent space (The tangent space is the locally flat neighbourhood of the momentary domain position, where effects of curvature can be still neglected.) to the vesicle the mean square displacement r^2 grows linearly with the time lag Δt as

$$r^2 = R^2\gamma^2 = 4R^2 D_{rot}\Delta t = 4D_{trans}\Delta t \qquad \text{for } \Delta t \to 0. \tag{3.5}$$

Equation (3.5) is the standard two-dimensional 'translational' diffusion law with the apparent 'translational' diffusion constant $D_{trans} = R^2 D_{rot}$. The apparent 'translational' diffusion defined in this way contains both the 'diffusion' of the domain in the membrane as well as the rigid rotational diffusion of the entire vesicle. For the rotational correlation function fitted in figure 3 we obtain the corresponding apparent 'translational' diffusion constant as $D_{trans} = 2.7\times 10^{-13}\,\mathrm{m^2\,s^{-1}}$. The conical angle θ is given by $\sin\theta = a/R$ (see figure 1). It measures the size of the domain in units of the size of the vesicle. Since the diffusion is due to thermal fluctuations then the rotational diffusion constant D_{rot} is related to the dimensionless friction coefficient f via the fluctuation dissipation theorem (Reichl 1980):

$$\frac{\eta_o R^3 \sin\theta}{k_B T} D_{rot} = \frac{1}{f}. \tag{3.6}$$

For the rotational diffusion constant fitted in figure 3 we obtain $f^{-1} = 4.2\times 10^{-2}$. The dimensionless friction coefficient

$$f = \frac{1}{\eta_o R^3 \sin\theta}\frac{\tau}{\omega} \tag{3.7}$$

is defined as the response in viscous torque τ of the domain when it is rotated with angular frequency ω. The dimensionless friction coefficient $f(\theta, \mathscr{H}, \mathscr{B}, \mathscr{H}_s)$ is a function of four dimensionless parameters: the conic angle θ of the domain, the relative bulk viscosity contrast $\mathscr{H} = (\eta_i - \eta_o)/\eta_o$ between the interior viscosity η_i and the exterior bulk fluid viscosity η_o of the vesicle, the Boussinesq number

$$\mathscr{B} = \eta_s^b/2\eta_o a \tag{3.8}$$

and the contrast $\mathscr{H}_s = (\eta_s^a - \eta_s^b)/\eta_s^b$ between the domain shear viscosity η_s^a and the surface shear viscosity η_s^b of the membrane embedding the domain. The dimensionless friction coefficient can be computed by solving the Stokes equation of the coupled bulk and membrane fluids. We will show in § 4 that a relatively simple analytic result exists for the special case $\mathscr{H}_s = 0$, where both bilayer phases have the same surface shear viscosity η_s. Once the analytic expression for the dimensionless friction coefficient is known, we can compare the dimensionless diffusion coefficient f^{-1} obtained from the experiment via (3.6) with the theoretical expression and extract the Boussinesq number $\mathscr{B}$ (and hence the surface shear viscosity η_s). As will be described in § 4 for

$\mathscr{H}_s = 0$ we obtain

$$\frac{1}{f} = \sum_{n=1}^{\infty} \frac{P_n^1(\cos\theta)^2}{2\pi \sin\theta n^2(n+1)^2[1 + \dfrac{n-1}{2n+1}(\mathscr{H} + 2(n+2)\mathscr{B}\sin\theta)]}, \tag{3.9}$$

where $P_n^1(\cos\theta)$ denotes the associated Legendre polynomial of the first kind of degree n and order 1. The sum in (3.9) quickly converges if the conic angle of the domain is large, and truncation of the sum at $n = 100$ gives results with errors less than 5 % for $\theta > \pi/20$. We may read off the value of the Boussinesq number from a plot of (3.9) versus $\mathscr{B}$ by looking at which Boussinesq number $\mathscr{B}$ the theoretical diffusion coefficient equation (3.9) coincides with the experimental diffusion coefficient equation (3.6) $f_{theory}^{-1}(\mathscr{B}) = f_{experiment}^{-1}$. The surface shear viscosity is then obtained via (3.8).

We define the sensitivity of the rheological method as

$$S = \frac{\mathrm{d}\ln f}{\mathrm{d}\ln \mathscr{B}}. \tag{3.10}$$

The sensitivity S expresses how much a relative change in viscosity $\Delta\eta_s/\eta_s$ will be reflected in a relative change in diffusion constant $\Delta D/D$. If the diffusion constant does not change significantly with the surface shear viscosity, then one cannot measure the surface shear viscosity to a high accuracy. This is indeed the case in single-domain rheology at both low and high Boussinesq numbers. At low Boussinesq number the diffusion of a single domain is dominated by the dissipation to the water and hence fairly independent of the surface shear viscosity. The same is true for high surface shear viscosity, where the vesicle performs rotational diffusion almost like a solid sphere. Only in the cross-over regime $1 < \mathscr{B} < 1/\sin\theta$ does one achieve significant sensitivity to allow a precise measurement of the surface shear viscosity.

We define the resolution limit of the method as $D_{res} = \Delta x_{min}^2/R^2\Delta t_{max}$ where Δx_{min} is the spatial resolution of the microscope and Δt_{max} is the maximum time of the measurement. The time limit for the measurement in one- and two-domain rheology is set by the time the domain will stay in the focus of the microscope which is given by $\Delta t_{max} = D_{rot}^{-1}$. We find that $D_{res} = \Delta x_{min}^2/R^2 D_{rot}$. Since the spatial resolution is smaller than the vesicle size, $\Delta x_{min} < R$ also the rotational diffusion constant is above the resolution limit $D_{res} < D_{rot}$. We then define the resolution of a diffusion constant as

$$Res = \frac{D}{D_{res}} = \frac{R^2}{\Delta x_{min}^2}\frac{D}{D_{rot}}. \tag{3.11}$$

A high resolution corresponds to $Res > 1$. A diffusion constant cannot be resolved when $Res < 1$. The resolution of single-domain rheology is $Res = R^2/\Delta x_{min}^2 \approx (20\,\mu\mathrm{m}/0.5\,\mu\mathrm{m})^2 \approx 10^3$. In order to detect the surface shear viscosity one needs both sensitivity and resolution. We define the measurability by

$$M = Res \times S. \tag{3.12}$$

The higher the measurability the easier it is to obtain a value for the surface shear viscosity.

4. Two-domain rheology: experiment

One-domain rheology has the disadvantage to be sensitive to the surface shear viscosity of the vesicle membrane only in the cross-over region $1 < \mathscr{B} < 1/\sin\theta$ since

at higher Boussinesq numbers the apparent diffusion of the domain is mainly due to rotations of the entire vesicle. These rotations dissipate the vesicle energy by shearing the surrounding bulk liquid not the membrane. One might eliminate the solid rotation by measuring the relative motion of two or more domains on the vesicle. Such measurements are indeed possible and two-particle microrheology has been used successfully with colloidal particles. The mathematics of two-particle rheology (Prasad *et al.* 2006), however, significantly differs from the results for one particle even when the system is flat rather than curved. Hydrodynamic interactions between two domains lead to correlated motion of the domains. Their relative motion is generally not the result of an independent motion of the single domains. Differences in the motion arising from hydrodynamic correlations (Levine & MacKintosh 2002; Fischer 2003) compared to an uncorrelated motion are especially large at large Boussinesq numbers $\mathscr{B} > \gamma/2\theta$ where γ denotes the angular separation of the two domains. Under these circumstances, hydrodynamic correlations are mediated by long range interfacial hydrodynamic interactions. Each domain has two degrees of freedom to move in the membrane giving rise to four normal modes of diffusion. For equally sized domains $a_1 = a_2$ symmetry considerations let us recognize those normal modes as the combined and relative motion of both domains along and perpendicular to the geodesics connecting both domains (figure 1). In § 4 we will derive equations connecting the Brownian angular velocity of all four modes with the corresponding Brownian torques at the domain edges. Numerical solution of the equations yields the combined and relative diffusion coefficients $f^{-1}_{comb,\parallel}$, $f^{-1}_{rel,\parallel}$, $f^{-1}_{comb,\perp}$ and $f^{-1}_{rel,\perp}$ parallel and perpendicular to the geodesic connecting the domain centres of the two domains. Diffusion of both domains will result in a change in separation γ. Since all four diffusion coefficients depend on the separation γ, a linear relation between the mean square displacement and time ($\gamma^2 \propto \Delta t$) will no longer hold over times allowing for significant change in γ. In a two-domain rheology experiment, the experimental data will be the vectors $\boldsymbol{c}_1(t)$ and $\boldsymbol{c}_2(t)$ describing the position of the two domains on the vesicle. We define the vector $\boldsymbol{c}_3(t)$ as $\boldsymbol{c}_3(t) = R\boldsymbol{c}_1 \times \boldsymbol{c}_2/|\boldsymbol{c}_1 \times \boldsymbol{c}_2|$. The vectors $\boldsymbol{c}_1(t)$, $\boldsymbol{c}_2(t)$ and $\boldsymbol{c}_3(t)$ define a basis for the three-dimensional space. The momentary angular velocities of both domains are

$$\boldsymbol{\omega}_1 = \frac{1}{R^2}\boldsymbol{c}_1 \times \frac{\mathrm{d}\boldsymbol{c}_1}{\mathrm{d}t} \qquad \text{and} \qquad \boldsymbol{\omega}_2 = \frac{1}{R^2}\boldsymbol{c}_2 \times \frac{\mathrm{d}\boldsymbol{c}_2}{\mathrm{d}t}. \tag{4.1}$$

We introduce a reciprocal basis as

$$\boldsymbol{q}_i = \frac{1}{2}\epsilon_{ijk}\frac{\boldsymbol{c}_j \times \boldsymbol{c}_k}{|(\boldsymbol{c}_1 \times \boldsymbol{c}_2)\cdot \boldsymbol{c}_3|}, \tag{4.2}$$

where ϵ_{ijk} denotes the Levi-Civita symbol. The vectors $\boldsymbol{c}_1$, $\boldsymbol{q}_2$ and $\boldsymbol{q}_3$ are orthogonal to each other and the vectors $\boldsymbol{q}_2$ and $\boldsymbol{q}_3$ span the tangent space to the domain located at the position $\boldsymbol{c}_1$. The same is true for the vectors $\boldsymbol{c}_2$, $\boldsymbol{q}_3$ and $\boldsymbol{q}_1$. The reciprocal vectors $\boldsymbol{q}_3$ and $\boldsymbol{q}_1$ span the tangent space to the domain located at the position $\boldsymbol{c}_2$. We decompose the angular velocities of both domains into combined and relative angular velocities parallel and perpendicular to the interconnecting geodesics between both domains via

$$\left.\begin{aligned} \boldsymbol{\omega}_1 &= \frac{\omega_{comb,\parallel} + \omega_{rel,\parallel}}{\sqrt{2}}\frac{\boldsymbol{q}_3}{|q_3|} + \frac{\omega_{comb,\perp} + \omega_{rel,\perp}}{\sqrt{2}}\frac{\boldsymbol{q}_2}{|q_2|}, \\ \boldsymbol{\omega}_2 &= \frac{\omega_{comb,\parallel} - \omega_{rel,\parallel}}{\sqrt{2}}\frac{\boldsymbol{q}_3}{|q_3|} - \frac{\omega_{comb,\perp} - \omega_{rel,\perp}}{\sqrt{2}}\frac{\boldsymbol{q}_1}{|q_1|}. \end{aligned}\right\} \tag{4.3}$$

Note that there is no component of $\boldsymbol{\omega}_1$ along $\boldsymbol{c}_1$ and no component of $\boldsymbol{\omega}_2$ along $\boldsymbol{c}_2$. This is because a 'rotation' of domain 1 around $\boldsymbol{c}_1$ leaves both the position and the shape of the domain unchanged and cannot be detected by the microscope. Note also that the rotations perpendicular to the connecting geodesic are around different axes ($\boldsymbol{q}_2$ and $\boldsymbol{q}_1$) for domains 1 and 2. It is straightforward to resolve (4.3) for the combined and relative angular velocities $\omega_{comb,\parallel}$, $\omega_{rel,\parallel}$, $\omega_{comb,\perp}$ and $\omega_{rel,\perp}$ as

$$\left.\begin{aligned}
\omega_{comb,\parallel} &= \frac{|q_3|}{\sqrt{2}}(\boldsymbol{\omega}_1 + \boldsymbol{\omega}_2)\cdot\boldsymbol{c}_3,\\
\omega_{rel,\parallel} &= \frac{|q_3|}{\sqrt{2}}(\boldsymbol{\omega}_1 - \boldsymbol{\omega}_2)\cdot\boldsymbol{c}_3,\\
\omega_{comb,\perp} &= \frac{\boldsymbol{\omega}_1\cdot\boldsymbol{c}_2|q_2| - \boldsymbol{\omega}_2\cdot\boldsymbol{c}_1|q_1|}{\sqrt{2}},\\
\omega_{rel,\perp} &= \frac{\boldsymbol{\omega}_1\cdot\boldsymbol{c}_2|q_2| + \boldsymbol{\omega}_2\cdot\boldsymbol{c}_1|q_1|}{\sqrt{2}}.
\end{aligned}\right\} \tag{4.4}$$

From (4.3) and (4.4) we obtain the relative velocity $\boldsymbol{u}_{1,rel}$ and $\boldsymbol{u}_{2,rel}$ between both domains at the position of domains 1 and 2:

$$\left.\begin{aligned}
\boldsymbol{u}_{1,rel} &= \sqrt{2}\omega_{rel,\parallel}\frac{\boldsymbol{c}_1\times\boldsymbol{q}_3}{|q_3|} + \sqrt{2}\omega_{rel,\perp}\frac{\boldsymbol{c}_1\times\boldsymbol{q}_2}{|q_2|},\\
\boldsymbol{u}_{2,rel} &= -\sqrt{2}\omega_{rel,\parallel}\frac{\boldsymbol{c}_2\times\boldsymbol{q}_3}{|q_3|} - \sqrt{2}\omega_{rel,\perp}\frac{\boldsymbol{c}_2\times\boldsymbol{q}_1}{|q_1|},
\end{aligned}\right\} \tag{4.5}$$

where $\boldsymbol{u}_{1,rel}$ and $\boldsymbol{u}_{2,rel}$ are 'relative' velocities in the sense of a two-dimensional non-Euclidian geometry on the vesicle surface. They are different from the Euclidian three-dimensional relative velocity $\mathrm{d}\boldsymbol{c}_1/\mathrm{d}t - \mathrm{d}\boldsymbol{c}_2/\mathrm{d}t$ that usually will not be tangential to the sphere. The 'relative' velocity $\boldsymbol{u}_{1,rel}$ is obtained in the following way. First, 'parallel' transport (Misner, Thorne & Wheeler 1973) of the velocity $\mathrm{d}\boldsymbol{c}_2/\mathrm{d}t$ from the position of domain 2 towards the domain 1 along the interconnecting geodesic will result in a velocity $\tilde{\boldsymbol{u}}_2$. This allows mapping of the velocity $\mathrm{d}\boldsymbol{c}_2/\mathrm{d}t$ of domain 2 defined in the tangent space of domain 2 into the tangent space of domain 1. In curved space such 'parallel' transport is necessary since vectors can be compared only when residing in the same tangent space. Only after this 'parallel' transport is achieved can the velocity $\tilde{\boldsymbol{u}}_2$ be subtracted from the velocity $\mathrm{d}\boldsymbol{c}_1/\mathrm{d}t$ of domain 1 to yield the 'relative' velocity $\mathrm{d}\boldsymbol{c}_1/\mathrm{d}t - \tilde{\boldsymbol{u}}_2$ evaluated in the tangent space of domain 1. Measurements of 'relative' velocities in curved space are usually quite difficult. We have taken advantage of the fact that the curved surface of the vesicle is embedded into a Euclidian three-dimensional space which made the computation of the 'relative' velocities in (4.5) much simpler than when performing the same operation in an arbitrarily curved space. 'Parallel' transport is just a rotation around the vector $\boldsymbol{c}_3$ by the angle γ. The difference between relative velocity in three-dimensional space and 'relative' velocity on a curved surface can be most easily understood when considering two domains, one sitting at the north pole and the other sitting at the south pole. Assume that both domains start moving 'towards' each other along the same longitude with the same velocities ($\mathrm{d}\boldsymbol{c}_1/\mathrm{d}t = \mathrm{d}\boldsymbol{c}_2/\mathrm{d}t$). The difference in velocities in three-dimensional space is zero. It makes sense in a two-dimensional curved space to speak of a 'relative' motion 'towards' each other and to measure a 'relative' velocity that will be just ($\mathrm{d}\boldsymbol{c}_1/\mathrm{d}t + \mathrm{d}\boldsymbol{c}_2/\mathrm{d}t$) not ($\mathrm{d}\boldsymbol{c}_1/\mathrm{d}t - \mathrm{d}\boldsymbol{c}_2/\mathrm{d}t$) . The plus sign instead of the minus sign arises because 'parallel' transport (a three-dimensional rotation of π in the three-dimensional

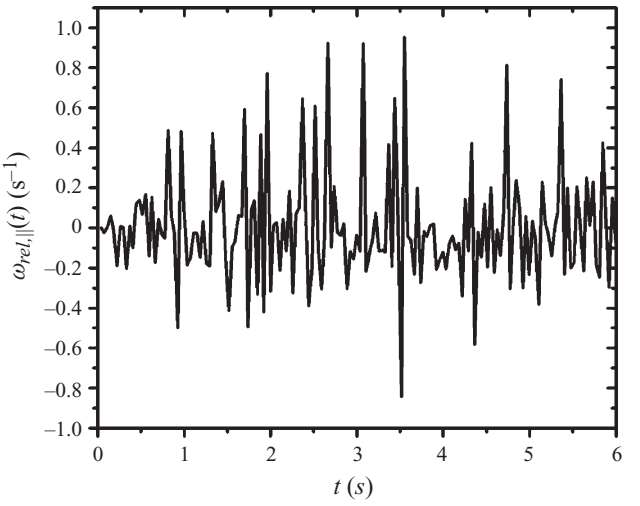

FIGURE 4. Plot of the relative longitudinal angular frequency $\omega_{rel,\parallel}(t)$ versus time of two domains with sizes $a_1 = 1.3\,\mu\text{m} \approx a_2 = 1.0\,\mu\text{m}$ separated by an angle of $\gamma = 30^\circ$ and residing in a vesicle of size $R = 12.5\,\mu\text{m}$ and composition (DOPC/DPPC/Chol = 16/64/20) at temperature $T = 23^\circ\text{C}$.

Euclidian sense) of the velocity of the domain at the south pole 'towards' the north pole just reverses the sign of the velocity.

Experimental measurements using two-domain rheology must average the angular velocity correlations

$$D_\lambda = \int_0^\infty \mathrm{d}\Delta t \langle \omega_\lambda(\gamma, t)\omega_\lambda(\gamma, t + \Delta t)\rangle \tag{4.6}$$

for each separation γ and each mode $\lambda = (comb, \parallel)$, $(rel, \parallel)$, $(comb, \perp)$ and $(rel, \perp)$ individually. Since the diffusion of each mode is due to thermal fluctuations the diffusion constants D_λ are related to the corresponding friction coefficients via the fluctuation dissipation theorem:

$$\frac{\eta_o R^3 \sin\theta}{k_B T} D_\lambda = \frac{1}{f_\lambda}, \tag{4.7}$$

where the friction coefficients describe the response in the viscous torque τ_λ,

$$f_\lambda = \frac{1}{\eta_o R^3 \sin\theta} \frac{\tau_\lambda}{\omega_\lambda}, \tag{4.8}$$

arising due to a rotation of both domains with frequency $\boldsymbol{\omega}_1(\lambda)$ and $\boldsymbol{\omega}_2(\lambda)$ and where the viscous torque has been decomposed into normal modes in a way analogous to the decomposition of frequencies equation (4.3). The normalization factors in (4.3) ensures that the power dissipated by the relative motion of both domains is

$$\langle \tau_\lambda(\gamma, t)\omega_\lambda(\gamma, t')\rangle = k_B T \delta(t - t'). \tag{4.9}$$

In figure 4 we depict the behaviour of the relative longitudinal angular frequency $\omega_{rel,\parallel}(t)$ of two domains with sizes $a_1 = 1.3\,\mu\text{m} \approx a_2 = 1.0\,\mu\text{m}$ separated by an angle of $\gamma = 30^\circ$ and residing in a vesicle of size $R = 12.5\,\mu\text{m}$ consisting of composition

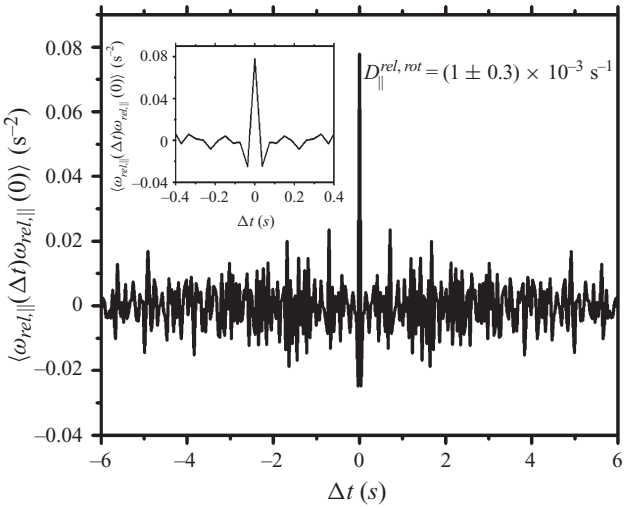

FIGURE 5. Plot of the auto correlation function $\langle \omega_{rel,\parallel}(\gamma, t)\omega_{rel,\parallel}(\gamma, t + \Delta t)\rangle$ computed from the data in figure 4. The diffusion constant $D_{rel,\parallel} = 1 \times 10^{-3}\ \mathrm{s}^{-1}$ corresponds to half the area under the auto correlation function. The region of the peak of the autocorrelation function at $\Delta t \approx 0$ that contributes to the diffusion is depicted with higher resolution in the inset.

(DOPC/DPPC/Chol = 16/64/20) at temperature $T = 23°\mathrm{C}$. The relative longitudinal angular frequency fluctuates around zero and does not change the separation γ by a significant amount during the time of measurement. The autocorrelation function $\langle \omega_{rel,\parallel}(\gamma, t)\omega_{rel,\parallel}(\gamma, t + \Delta t)\rangle$ is depicted in figure 5. The diffusion constant $D_{rel,\parallel}$ corresponds to half the area under the correlation function. Like the angular frequency, torque correlation in (4.9), also the angular frequency autocorrelation function, is delta correlated. The fluctuations persisting in figure 5 are due to the limited time of measurement and the integration in (4.6) is therefore taken over a time span of three frames, e.g. larger than the correlation time but smaller than the time of measurement.

Only the relative longitudinal motion of the domains results in a motion where the vesicle as a whole is at rest. Transversal relative motion results in a net rotation of the vesicle around the midpoint between both domains. Separation of relative and global motion of the vesicle therefore remains incomplete also for two-domain rheology. On a curved surface, combined motion into one direction means that the direction of the first domain is the same as the second after that the second direction is parallel transported (Misner *et al.* 1973) along the interconnecting geodesics to the first domain. The combined motion of both domains is the analogue of one domain rheology with two domains. The analysis of the two-domain rheology consists of the decomposition of the motion into the four modes and a measurement of the autocorrelation function of the angular velocity fluctuations of a particular mode, (4.6) at a fixed separation of domains. The diffusion constant of the particular mode is obtained from the ensemble and time average over these fluctuations. Again a comparison between the theoretical diffusion coefficients $f_{\lambda}^{-1}(\theta, \gamma, \mathscr{B})$ and the four different experimental diffusion constants determined from (4.7) allows extraction of the Boussinesq number and using (3.8), the surface shear viscosity. As described in §4 for $\mathscr{H}_s = 0$ and $\gamma = \pi$ two of the four modes become degenerate and we

obtain:

$$\left.\begin{aligned}\frac{1}{f_{rel,\parallel}} = \frac{1}{f_{comb,\perp}} &= 2\sum_{n=2,4,6\ldots}^{\infty} \frac{P_n^1(\cos\theta)^2}{2\pi\sin\theta n^2(n+1)^2[1+\dfrac{n-1}{2n+1}(\mathscr{H}+2(n+2)\mathscr{B}\sin\theta)]},\\ \frac{1}{f_{rel,\perp}} = \frac{1}{f_{comb,\parallel}} &= 2\sum_{n=1,3,5\ldots}^{\infty} \frac{P_n^1(\cos\theta)^2}{2\pi\sin\theta n^2(n+1)^2[1+\dfrac{n-1}{2n+1}(\mathscr{H}+2(n+2)\mathscr{B}\sin\theta)]}.\end{aligned}\right\} \tag{4.10}$$

The sum for the two domains in (4.10) differs from the corresponding equation (3.9) of a single domain in several aspects. The summation in (4.10) is only over odd (even) values of n. The summation quickly converges if the conic angle of both domains and the separation angle $2(\pi/2-\theta)$ are large. Moreover truncation of the sum at $n=100$ gives results with errors less than 5 % for $\theta > \pi/20$ and $2(\pi/2-\theta) > \pi/20$. We may estimate the value of the Boussinesq number from a plot of (4.10) versus $\mathscr{B}$ by looking where the theoretical diffusion coefficient of (4.10) equals the experimental diffusion coefficient determined from (4.7). The surface shear viscosity is then obtained via (3.8). The advantage of two-domain rheology with respect to one-domain rheology is that in some of the modes one gains sensitivity for the surface shear viscosity. One disadvantage is that such technique requires to statistically average the angular velocity correlations for a subset of events, where the domains have similar separation. Moreover, at high surface shear viscosity the rotational diffusion of the vesicle in the water is much faster than the relative diffusion of two domains. The time to observe these domains with high spatial resolution is limited by $\Delta t_{max} \approx D_{rot}^{-1}$ since for longer times both domains, which are originally located on the northern hemisphere of the vesicle, will diffuse to the southern hemisphere via the rotational diffusion of the entire vesicle and therefore be out of the focal plane of the objective. For large Boussinesq numbers, relative diffusion D_{rel} will eventually drop below the diffusion resolution limit $D_{rel} < D_{res}$. In two-domain rheology one will gain the missing sensitivity at high Boussinesq numbers using the relative longitudinal mode but will lose resolution in the measurement of the relative diffusion constants as compared to the high resolution of measuring rotational diffusion constants with single-domain rheology.

5. Theoretical

In this section we outline the derivation of the single-domain diffusion constant equation (3.9) and the two-domain diffusion constants equation (4.10). The bulk liquid inside and outside the vesicle fulfills the Stokes equation:

$$\left.\begin{aligned}-\nabla p + \eta\Delta\boldsymbol{u} &= 0,\\ \nabla\cdot\boldsymbol{u} &= 0.\end{aligned}\right\} \tag{5.1}$$

Here $\boldsymbol{u}$ is the bulk fluid velocity. The dynamic bulk ($\boldsymbol{P}$) and surface ($\boldsymbol{P}_s$) stress tensors are given by

$$\left.\begin{aligned}\boldsymbol{P} &= -p\mathbf{1} + \eta\left(\nabla\boldsymbol{u} + [\nabla\boldsymbol{u}]^t\right),\\ \boldsymbol{P}_s &= \sigma_s\boldsymbol{I}_s + \eta_s\left(\nabla_s\boldsymbol{u}_s\cdot\boldsymbol{I}_s + \boldsymbol{I}_s\cdot[\nabla_s\boldsymbol{u}_s]^t\right),\end{aligned}\right\} \tag{5.2}$$

where p is the bulk pressure, η is the bulk viscosity, σ_s is the surface tension and η_s is the surface shear viscosity. The index s is used for quantities defined at the vesicle

surface. They are obtained from the corresponding bulk quantities by projection onto the tangent space of the vesicle using the surface idem factor $\boldsymbol{I}_s = \mathbf{1} - \boldsymbol{nn}$, where $\boldsymbol{n}$ is the normal vector to the vesicle surface (i.e. $\boldsymbol{u}_s = \boldsymbol{I}_s \cdot \boldsymbol{u}$, $\nabla_s = \boldsymbol{I}_s \cdot \nabla$). To compute the resistance of the domain to the action of an external force we assume an external surface force density $\boldsymbol{f}_s$ distributed around the edge of the domain (figure 1). The vesicle surface is assumed incompressible and the divergence of the dynamic surface tension tensor is balanced by the traction $\boldsymbol{n} \cdot \|\boldsymbol{P}\| \cdot \boldsymbol{I}_s$ from the two bulk liquids and by the surface force density:

$$\left.\begin{array}{c} \boldsymbol{n} \cdot \|\boldsymbol{P}\| \cdot \boldsymbol{I}_s = \boldsymbol{f}_s + \nabla_s \cdot \boldsymbol{P}_s, \\ \nabla_s \cdot \boldsymbol{u}_s = 0. \end{array}\right\} \tag{5.3}$$

Here $\|\boldsymbol{P}\|$ denotes the discontinuity of the bulk stress tensor across the vesicle interface. In general, the vesicle interior might have different properties than the exterior and we denote the velocities inside and outside the vesicle by $\boldsymbol{u}_i$ and $\boldsymbol{u}_o$. η_i and η_o are the bulk viscosities inside and outside the vesicle. In general, we also will have two surface viscosities, one for the domain η_s^a and one η_s^b for the rest of the membrane. We have so far discussed the rheological properties of the bulk fluid and the membrane. Of course there are also the rheological properties of the one-dimensional boundary between the portion of the membrane within the domain and the rest of the membrane. A one-dimensional line cannot be sheared and there is no analogue to the shear viscosities of the membrane and the bulk on the domain edge. However, the presence or absence of linactants (Trabelsi *et al.* 2006) (molecules that preferentially adsorb to the domain edge) will have a pronounced effect on the line compressibility and the line dilatational viscosity of the edge. The general line stress tensor would hence read

$$\boldsymbol{P}_l = (\sigma_l + \eta_l^{dil} \nabla_l \cdot \boldsymbol{u}_l) \boldsymbol{I}_l \tag{5.4}$$

with σ_l the line tension, η_l^{dil} the line dilatational viscosity, $\boldsymbol{I}_l$ the line idem factor, ∇_l the line gradient and $\boldsymbol{u}_l$ the line velocity. The Stokes equation for the line edge then reads

$$\boldsymbol{n}_l \cdot \|\boldsymbol{P}_s\| \cdot \boldsymbol{I}_l = \nabla_l \cdot \boldsymbol{P}_l, \tag{5.5}$$

where $\|\boldsymbol{P}_s\|$ denotes the discontinuity of the surface stress tensor across the edge of the domain. The equation of continuity reads

$$\nabla_l \cdot (\rho_l \boldsymbol{u}_l) = 0 \tag{5.6}$$

with ρ_l the linactant line density at the domain edge. A closure of the equations requires a constitutive equation for the line tension $\sigma_l(\rho_l)$. Little is known about the presence or absence of linactants, and even less is known about their compressibility and dilatational viscosity. Fluorescently labelled molecules sometimes act as linactants. Here we will assume a free domain edge without linactants $\rho_l = 0$ and $\eta_l^{dil} = 0$ such that $\nabla_l \sigma_l = 0$. For a free domain edge all rheological properties of the domain edge vanish and we find that all domain edge forces parallel to the domain edge vanish. We will hence assume that the surface force $\boldsymbol{f}_s$ in (5.3) is concentrated at the domain edge and pointing normal to the domain edge.

We will solve the problem in several steps. Firstly, we reduce the vector equations to scalar equations. In the second step, the relations between the torque and the velocities are reduced to equations solely involving velocities and torques on the vesicle surface. The third step reduces the relations to the velocity and torque fields on the domain edges. The equations on the domain edge are one-dimensional and can therefore be solved in a straightforward way.

We impose spherical coordinates r, ϑ and φ centred in the vesicle with the corresponding unit vectors $\boldsymbol{e}_r$, $\boldsymbol{e}_\vartheta$ and $\boldsymbol{e}_\varphi$. R is the radius of the vesicle.

The general solution of the bulk Stokes equation (5.1) can be written as

$$\boldsymbol{u} = \eta \int \mathrm{d}^3\boldsymbol{r}' \frac{\nabla p(\boldsymbol{r}')}{\boldsymbol{r}-\boldsymbol{r}'} + \nabla \Xi + (\nabla \times \boldsymbol{r})\Psi, \tag{5.7}$$

where p, Ξ and Ψ are scalar functions satisfying the Laplace equation $\nabla^2 p = \nabla^2 \Xi = \nabla^2 \Psi = 0$. Due to the incompressibility of the bulk velocity and the surface velocity on the vesicle, the flow can be described by the function Ψ only and $p = \Xi = 0$. It has been shown in the work of Saffmann & Delbrück (1975) that the incompressibility of the bulk and interfacial liquids causes all streamlines to be parallel to the interface and leads to a flow that is free of pressure gradients. This fact also holds when the interface is spherical and we therefore neglect the pressure gradients from the very beginning Fischer *et al.* (2006). The tangential stress-boundary condition (5.3) takes the form Edwards, Brenner & Wasan (1991):

$$-r\eta_o \frac{\partial \boldsymbol{u}_o/r}{\partial r} + r\eta_i \frac{\partial \boldsymbol{u}_i/r}{\partial r}\Bigg)_s = \boldsymbol{f}_s + \nabla_s \sigma_s + \eta_s \left\{ \boldsymbol{e}_r \times \nabla_s \left[(\nabla_s \times \boldsymbol{u}_s) \cdot \boldsymbol{e}_r \right] - \frac{2}{R^2} \boldsymbol{u}_s \right\}. \tag{5.8}$$

Using (5.7) and scalar multiplying (5.8) with $\boldsymbol{r} \times \nabla$ results in

$$-\nabla \cdot \boldsymbol{\tau}_s = \hat{\Lambda}_s \Psi, \tag{5.9}$$

where

$$\boldsymbol{\tau}_s = \boldsymbol{r} \times \boldsymbol{f}_s \tag{5.10}$$

denotes the surface torque density acting on the surface of the vesicle and $\hat{\Lambda}_s$ is the surface rheological operator:

$$\hat{\Lambda}_s \Psi = \left\| r \frac{\partial}{\partial r} r \nabla_s^2 \eta \Psi \right\|_{r=R} + \eta_s(\vartheta, \varphi) R^2 \nabla_s^2 \left(\nabla_s^2 + \frac{2}{R^2} \right) \Psi. \tag{5.11}$$

If we set the surface shear viscosity to be constant $\bar{\eta}_s = (\eta_s^a + \eta_s^b)/2$ over the entire vesicle membrane, the surface rheological operator $\bar{\hat{\Lambda}}_s = \hat{\Lambda}_s(\eta = \bar{\eta})$ commutes with the operator $\nabla \times \boldsymbol{r}$ and with the surface Laplace operator $\nabla_s^2 = (1/r^2)(\nabla \times \boldsymbol{r})^2$. It therefore follows that the functions

$$\left.\begin{aligned} \Psi_{nm}^e &= \begin{cases} \omega R \left(\dfrac{r}{R}\right)^n \cos(m\varphi) P_n^m(\cos\vartheta) & \text{for } r < R, \\ \omega R \left(\dfrac{R}{r}\right)^{n+1} \cos(m\varphi) P_n^m(\cos\vartheta) & \text{for } r > R, \end{cases} \\ \Psi_{nm}^o &= \begin{cases} \omega R \left(\dfrac{r}{R}\right)^n \sin(m\varphi) P_n^m(\cos\vartheta) & \text{for } r < R, \\ \omega R \left(\dfrac{R}{r}\right)^{n+1} \sin(m\varphi) P_n^m(\cos\vartheta) & \text{for } r > R, \end{cases} \end{aligned}\right\} \tag{5.12}$$

are simultaneous eigenfunctions of the three operators $\bar{\hat{\Lambda}}_s$, $\nabla \times \boldsymbol{r}$ and ∇_s^2. We will only solve problems that are mirror symmetric with respect to the operation $\varphi \to -\varphi$ and hence the solution will involve only the even functions Ψ_{nm}^e or only the odd functions Ψ_{nm}^o. We describe the solution for the even functions and will omit the index e in Ψ_{nm}^e, wherever the equation holds in the same way for the odd solutions. The

functions $P_n^m(\cos\vartheta)$ are associated Legendre polynomials. The eigenvalue equation for the operator $\bar{\hat{\Lambda}}_s$ on the vesicle surface reads

$$\bar{\hat{\Lambda}}_s \Psi_{nm} = \lambda_n \Psi_{nm} \tag{5.13}$$

with

$$\lambda_n = \eta_o R^{-1} n(n+1)\left[2n+1+(n-1)\left\{\mathscr{H}+2(n+2)(1+\mathscr{H}_s/2)\mathscr{B}\sin\theta\right\}\right]. \tag{5.14}$$

In the case that the membrane surface shear viscosity differs inside and outside the domain we write the surface shear viscosity as

$$\eta_s = 2\eta_o R\mathscr{B}\sin\theta\,[1+\mathscr{H}_s/2(1+\chi(\vartheta,\varphi))], \tag{5.15}$$

where the function $\chi(\vartheta,\varphi)$ is equal to ± 1 depending on whether (ϑ,φ) is a point inside or outside the domains:

$$\chi = \begin{cases} +1 & \text{for } \vartheta,\varphi \in \text{ domains,} \\ -1 & \text{for } \vartheta,\varphi \notin \text{ domains.} \end{cases} \tag{5.16}$$

We write the surface rheological operator as $\hat{\Lambda}_s = \bar{\hat{\Lambda}}_s + \chi(\vartheta,\varphi)\delta\hat{\Lambda}_s$. While the operators $\bar{\hat{\Lambda}}_s$ and $\delta\hat{\Lambda}_s$ commute with $\nabla\times\boldsymbol{r}$ and ∇_s^2, the operator $\hat{\Lambda}_s$ does not commute with $\nabla\times\boldsymbol{r}$ and ∇_s^2. We define the scalar product

$$\langle f, g\rangle = \int R^2 \sin\vartheta\,\mathrm{d}\vartheta\,\mathrm{d}\varphi f^*(\vartheta,\varphi) g(\vartheta,\varphi). \tag{5.17}$$

With the scalar product equation (5.17) the functions Ψ_{nm} are orthogonal and one has

$$\langle \Psi_{\tilde{n}\tilde{m}}, \Psi_{nm}\rangle = N_{\tilde{n}\tilde{m}}\delta_{\tilde{n}n}\delta_{\tilde{m}m} \tag{5.18}$$

with normalization constant

$$N_{\tilde{n}\tilde{m}} = \omega^2 R^4 \frac{2\pi}{2\tilde{n}+1}\frac{\tilde{n}+\tilde{m}!}{\tilde{n}-\tilde{m}!} \quad \text{for} \quad \tilde{m}\neq 0. \tag{5.19}$$

Taking the scalar product of $\Psi_{\tilde{n}\tilde{m}}$ with (5.9) results in

$$\begin{aligned} -\langle \Psi_{\tilde{n}\tilde{m}}, \nabla_s\cdot\boldsymbol{\tau}_s\rangle = \langle \Psi_{\tilde{n}\tilde{m}}, \hat{\Lambda}_s\Psi\rangle &= \sum_{nm}\langle \Psi_{\tilde{n}\tilde{m}}, [\bar{\hat{\Lambda}}_s + \chi\delta\hat{\Lambda}_s]\Psi_{nm}\rangle \frac{1}{N_{nm}}\langle \Psi_{nm}, \Psi\rangle \\ &= \sum_{nm}\lambda_{\tilde{n}}\Delta_{\tilde{n}\tilde{m},nm}\langle \Psi_{nm}, \Psi\rangle, \end{aligned} \tag{5.20}$$

where

$$\Delta_{\tilde{n}\tilde{m},nm} = \left\{\delta_{\tilde{n}n}\delta_{\tilde{m}m} + \langle \Psi_{\tilde{n}\tilde{m}}, \frac{\chi\delta\hat{\Lambda}_s}{\lambda_{\tilde{n}}N_{\tilde{n}\tilde{m}}}\Psi_{nm}\rangle\right\} = \left\{\delta_{\tilde{n}n}\delta_{\tilde{m}m} + \frac{\delta\lambda_n}{\lambda_{\tilde{n}}}\frac{\langle \Psi_{\tilde{n}\tilde{m}}, \chi(\vartheta,\varphi)\Psi_{nm}\rangle}{N_{\tilde{n}\tilde{m}}}\right\} \tag{5.21}$$

and

$$\delta\lambda_n = \eta_o R^{-1}(n-1)n(n+1)(n+2)\mathscr{H}_s\mathscr{B}\sin\theta. \tag{5.22}$$

Inverting (5.20) results in

$$\langle \Psi_{nm}, \Psi\rangle = -\sum_{\tilde{n}\tilde{m}}(\Delta^{-1})_{nm,\tilde{n}\tilde{m}}\frac{\langle \Psi_{\tilde{n}\tilde{m}}, \nabla_s\cdot\boldsymbol{\tau}_s\rangle}{\lambda_{\tilde{n}}}. \tag{5.23}$$

For a given torque density $\boldsymbol{\tau}_s$ on the vesicle we find the corresponding velocity profile as

$$\boldsymbol{u} = \sum_{nm} (\nabla \times \boldsymbol{r}) \Psi_{nm} \frac{\langle \Psi_{nm}, \Psi \rangle}{N_{\tilde{n}\tilde{m}}} = - \sum_{nm,\tilde{n}\tilde{m}} (\nabla \times \boldsymbol{r}) \Psi_{nm} (\Delta^{-1})_{nm,\tilde{n}\tilde{m}} \frac{\langle \Psi_{\tilde{n}\tilde{m}}, \nabla_s \cdot \boldsymbol{\tau}_s \rangle}{\lambda_{\tilde{n}} N_{\tilde{n}\tilde{m}}}. \tag{5.24}$$

We retain our freedom to place our domains of conical angle θ at an arbitrary latitude γ. It is therefore convenient to use an alternative system of spherical coordinates $(\vartheta_\gamma, \varphi_\gamma)$ with its pole centred in the domain at latitude γ. The transformation from coordinates (ϑ, φ) to $(\vartheta_\gamma, \varphi_\gamma)$ is then achieved via

$$\left.\begin{aligned} \vartheta &= \arccos(\cos\gamma \cos\vartheta_\gamma - \sin\gamma \sin\vartheta_\gamma \cos\varphi_\gamma), \\ \varphi &= \arctan \frac{\sin\varphi_\gamma}{\cos\gamma \cos\varphi_\gamma + \sin\gamma \cot\vartheta_\gamma}. \end{aligned}\right\} \tag{5.25}$$

The edge of the domain at latitude γ is then given by the equation $\vartheta_\gamma = \theta$. It is useful to define a second scalar product on the edge of the domain via

$$\{f, g\}_{\gamma,\theta} = \int_{-\pi}^{\pi} \frac{\mathrm{d}\varphi_\gamma}{\pi} f^*(\vartheta(\vartheta_\gamma = \theta, \varphi_\gamma), \varphi(\vartheta_\gamma = \theta, \varphi_\gamma)) g(\vartheta(\vartheta_\gamma = \theta, \varphi_\gamma), \varphi(\vartheta_\gamma = \theta, \varphi_\gamma)), \tag{5.26}$$

where the integral

$$\{\cos(\nu\phi_\gamma), \Psi^e_{nm}\}_{\gamma,\theta} = \int_{-\pi}^{\pi} \frac{\mathrm{d}\varphi_\gamma}{\pi} \cos(\nu\phi_\gamma) \Psi^e_{nm}(\vartheta(\vartheta_\gamma = \theta, \varphi_\gamma), \varphi(\vartheta_\gamma = \theta, \varphi_\gamma)) \tag{5.27}$$

denotes the Fourier cosine transform of the even eigenfunction Ψ^e_{nm} on the edge of the domain at latitude γ. Similarly, we find the Fourier coefficients of the normal velocity to the domain edge at latitude γ as

$$\left.\begin{aligned} \check{u}_{\vartheta_\gamma,\nu}[\gamma, \theta] &= \{\sin(\nu\varphi_\gamma), \boldsymbol{e}_{\vartheta_\gamma} \cdot (\nabla \times \boldsymbol{r}) \Psi\}_{\gamma,\theta} = -\{\boldsymbol{e}_{\vartheta_\gamma} \cdot (\nabla \times \boldsymbol{r}) \sin(\nu\varphi_\gamma), \Psi\}_{\gamma,\theta} \\ &= \frac{-\nu}{sin\theta} \{\cos(\nu\varphi_\gamma), \Psi\}_{\gamma,\theta} = - \sum_{nm} \nu \{\cos(\nu\varphi_\gamma), \Psi^e_{nm}\}_{\gamma,\theta} \frac{\langle \Psi^e_{nm} \Psi \rangle}{N_{nm} \sin\theta}, \\ &= \sum_{nm} \nu \{\cos(\nu\varphi_\gamma), \Psi^e_{nm}\}_{\gamma,\theta} (\Delta^{-1})_{nm,\tilde{n}\tilde{m}} \frac{\langle \Psi^e_{\tilde{n}\tilde{m}} \nabla_s \cdot \boldsymbol{\tau}_s \rangle}{\lambda_{\tilde{n}} N_{nm} \sin\theta}. \end{aligned}\right\} \tag{5.28}$$

We anticipate a surface torque density parallel to the edge of a second domain at the same longitude but different latitude $\tilde{\gamma}$ as

$$\boldsymbol{\tau}^e_s[\tilde{\gamma}, \theta] = \frac{\delta(\vartheta_{\tilde{\gamma}} - \theta) \boldsymbol{e}_{\varphi_{\tilde{\gamma}}}}{\pi R^2 \sin\theta} \sum_{\mu=1}^{\infty} \check{\tau}_\mu[\tilde{\gamma}, \theta] \sin(\mu\varphi_{\tilde{\gamma}}), \tag{5.29}$$

where the pre-factor is chosen such that the total torque on the second domain

$$|\boldsymbol{\tau}_{tot}| = \left| \int R^2 sin\vartheta_{\tilde{\gamma}} \, d\vartheta_{\tilde{\gamma}} \, \mathrm{d}\varphi_{\tilde{\gamma}} \boldsymbol{\tau}^e_s[\tilde{\gamma}, \theta] \right| = |\check{\tau}_1[\tilde{\gamma}, \theta]| \tag{5.30}$$

is given by the first Fourier coefficient $\check{\tau}_1[\tilde{\gamma}, \theta]$ of the second domain. We obtain

$$\left.\begin{aligned} \langle \Psi^e_{\tilde{n}\tilde{m}}, \nabla_s \cdot \boldsymbol{\tau}^e_s[\tilde{\gamma}, \theta] \rangle &= \int R^2 \sin\vartheta_{\tilde{\gamma}} \, \mathrm{d}\vartheta_{\tilde{\gamma}} \, \mathrm{d}\varphi_{\tilde{\gamma}} \Psi^{e*}_{\tilde{n}\tilde{m}} \frac{\boldsymbol{e}_{\varphi_{\tilde{\gamma}}}}{R \sin\theta} \cdot \frac{\partial \boldsymbol{\tau}^e_s[\tilde{\gamma}, \theta]}{\partial \varphi_{\tilde{\gamma}}} \\ &= \int \mathrm{d}\varphi_{\tilde{\gamma}} \Psi^{e*}_{\tilde{n}\tilde{m}} \sum_{\mu=1}^{\infty} \frac{\mu}{\pi R \sin\theta} \check{\tau}_\mu[\tilde{\gamma}, \theta] \cos(\mu\varphi_{\tilde{\gamma}}), \\ &= \frac{1}{R \sin\theta} \sum_{\mu=1}^{\infty} \mu \check{\tau}_\mu[\tilde{\gamma}, \theta] \{\Psi^e_{\tilde{n}\tilde{m}}, \cos(\mu\varphi_{\tilde{\gamma}})\}_{\tilde{\gamma},\theta}. \end{aligned}\right\} \tag{5.31}$$

Inserting (5.31) in (5.28) we find

$$\check{u}_{\vartheta_\gamma,\nu}[\gamma,\theta] = \sum_{\mu} O_{\nu\mu}[\gamma,\theta;\tilde{\gamma},\theta]\check{\tau}_{\mu}[\tilde{\gamma},\theta], \tag{5.32}$$

where

$$O_{\nu\mu}[\gamma,\theta;\tilde{\gamma},\theta] = \sum_{nm,\tilde{n}\tilde{m}} \frac{\nu\mu\{\cos(\nu\varphi_\gamma), \Psi^e_{nm}\}_{\gamma,\theta}(\Delta^{-1})_{nm,\tilde{n}\tilde{m}}\{\Psi^e_{\tilde{n}\tilde{m}}, \cos(\mu\varphi_{\tilde{\gamma}})\}_{\tilde{\gamma},\theta}}{R\sin^2\theta\lambda_{\tilde{n}}N_{nm}}. \tag{5.33}$$

The domain edge Oseen tensor $O_{\nu\mu}[\gamma,\theta;\tilde{\gamma},\theta]$ measures the response in the Fourier component of the normal velocity $\check{u}_{\vartheta_\gamma,\nu}[\gamma,\theta]$ on the edge of the domain centred at latitude γ to the Fourier component of the torque $\check{\tau}_\mu[\tilde{\gamma},\theta]$ on a different domain centred at latitude $\tilde{\gamma}$. Note that (5.32) requires the knowledge of the normal velocity field and torque density only at the edges of the domains. The normal velocities however are fixed via the specific mode of motion of the domains.

The computation of the single- and two-domain friction coefficients is now straightforward. We proceed with the computation of the single-domain friction first. Without loss of generality we may place the single domain at the north pole $\gamma = 0$. For this case the coordinates systems (ϑ,φ) and $(\vartheta_\gamma,\varphi_\gamma)$ coincide. We find

$$\{\cos(\nu\varphi_\gamma), \Psi_{nm}\}_{\gamma=0,\theta} = \omega R\delta_{nm}P_n^m(\cos\theta) \tag{5.34}$$

and

$$(\Delta)_{\tilde{n}\tilde{m},nm} = \delta_{\tilde{m}m}\Delta_{m,\tilde{n}n} \tag{5.35}$$

with

$$\Delta_{m,\tilde{n}n} = \left\{\delta_{\tilde{n}n} - \frac{\delta\lambda_n}{\lambda_{\tilde{n}}}\frac{\pi\omega^2R^4\int_{-1}^{1}\mathrm{d}x\ \mathrm{sign}(x-\cos\theta)P_{\tilde{n}}^m(x)P_n^m(x)}{N_{nm}}\right\}. \tag{5.36}$$

The Oseen tensor becomes diagonal in ν and μ. We require the domain to rotate with velocity $\boldsymbol{u} = \omega\boldsymbol{e}_y \times \boldsymbol{r}$ such that $\check{u}_{\vartheta,1} = \omega R$ and $\check{u}_{\vartheta,\nu} = 0$ for $\nu = 2, 3, \ldots$. This requires a torque $\check{\tau}_1 = \omega R/O_{11}$, and $\check{\tau}_\nu = 0$ for $\nu = 2, 3, \ldots$, with

$$O_{11}[0,\theta;0,\theta] = \sum_{n,\tilde{n}} \frac{\omega^2RP_n^1(\cos\theta)(\Delta_1{}^{-1})_{n,\tilde{n}}P_{\tilde{n}}^1(\cos\theta)}{\sin^2\theta\lambda_{\tilde{n}}N_{n1}}. \tag{5.37}$$

For the case $\mathscr{H}_s = 0$ the inversion of Δ is trivial and we regain (3.9) by noting that

$$\frac{1}{f} = \eta_o R^3\sin\theta\frac{\omega}{|\check{\tau}_1|} = \eta_o R^2\sin\theta O_{11}[0,\theta;0,\theta], \tag{5.38}$$

$$\mathscr{B} = \frac{\eta_s}{2\eta_o R\sin\theta} = \frac{\eta_s}{2\eta_o a} \tag{5.39}$$

is the Boussinesq number defined with the domain radius a. In the limit $\mathscr{B}\to\infty$ all terms except for $n = 1$ vanish in (5.37) and using (5.38) we find

$$\frac{1}{f}(\mathscr{B}\to\infty) = \sin\theta/8\pi, \tag{5.40}$$

which is the result for a rigid rotating sphere (Russel, Saville & Schowalter 1989) on the other hand small angles θ the sum in (5.37) converges only after summing over large numbers n. We may convert the sum into an integral and we might use the relation

$$\lim_{n\to\infty} n^{-m}P_n^m(\cos\vartheta) = \mathrm{J}_m(n\vartheta), \tag{5.41}$$

where $J_m(n\vartheta)$ is a Bessel function of order m. With these manipulations we rediscover the equation of De Koker (1996) for a flat membrane:

$$\frac{1}{f}(\mathscr{B}, \theta \to 0) = \frac{1}{2\pi}\int_0^\infty \mathrm{d}x \frac{J_1(x)^2}{x^2(1+\mathscr{B}x)} \overset{\mathscr{B}\to 0}{=} \frac{1}{2}\frac{4}{3\pi^2}. \tag{5.42}$$

Noting that the drag force is $F_{drag} = \check{\tau}_1/R$ and the domain velocity is $U_{Domain} = R\omega$ in a flat surface equation (5.42) predicts half of the result of De Koker (1996) for a flat monolayer domain having the same surface shear viscosity as the rest of the membrane. The factor 1/2 arises because we have a bilayer with water on both sides of the membrane. The theory of Hughes *et al.* (1981) for a rigid domain would be obtained for the case where one first performs the limit $\theta \to 0$ and afterwards the limit towards a solid domain $\mathscr{H}_s \to \infty$. The numerical inversion of the matrix Δ in (5.37) involves matrix elements with higher indices n and m that makes the evaluation more difficult the smaller the conical angle θ of the domain.

For the computation of the relative two-domain diffusion coefficient we consider the first domain to sit at the north pole and the second to sit at latitude γ . The latitude γ of the second domain must be larger than twice the conical angle of the domains $2\theta < \gamma < \pi$ for the domains not to overlap. For a relative motion of the domains we require the torques on one domain to be the inversion at the midpoint between both domains of the torque on the other domain: $\tau_{\varphi_0}[0,\theta](\varphi_0) = \tau_{\varphi_\gamma}[\gamma,\theta](\varphi_\gamma = \varphi_0 + \pi)$ which translates into

$$\check{\tau}_\mu[0,\theta] = (-1)^\mu \check{\tau}_\mu[\gamma,\theta]. \tag{5.43}$$

For a combined motion one finds $\check{\tau}_\mu[0,\theta] = (-1)^{\mu+1}\check{\tau}_\mu[\gamma,\theta]$. Here, we will derive the Oseen tensor for the relative motion. The velocity of the domain on the north pole occurs due to the torques from both domains and we find

$$\check{u}_{\vartheta,\nu}[0,\theta] = \sum_\mu \left(O_{\nu\mu}[0,\theta;0,\theta] + (-1)^\mu O_{\nu\mu}[0,\theta;\gamma,\theta]\right)\check{\tau}_\mu[0,\theta] = \sum_\mu O^{tot}_{\nu\mu}\check{\tau}_\mu[0,\theta], \tag{5.44}$$

where

$$O^{e,tot}_{\nu\mu} = \sum_{n,\tilde{n}\tilde{m}} \frac{\nu\mu\omega P_n^\nu(\cos\theta)(\Delta^{-1})_{n\nu,\tilde{n}\tilde{m}}[\omega R P^\mu_{\tilde{n}}(\cos\theta)\delta_{\tilde{m}\mu} + (-1)^\mu\{\Psi^e_{\tilde{n}\tilde{m}}, \cos(\mu\varphi_\gamma)\}]}{\sin^2\theta\lambda_{\tilde{n}}N_{n\nu}}. \tag{5.45}$$

The Oseen tensor for the odd solution is obtained by replacing $\{\Psi^e_{\tilde{n}\tilde{m}}, \cos(\mu\varphi_\gamma)\}$ with $\{\Psi^o_{\tilde{n}\tilde{m}}, \sin(\mu\varphi_\gamma)\}$ in (5.45):

$$O^{o,tot}_{\nu\mu} = \sum_{n,\tilde{n}\tilde{m}} \frac{\nu\mu\omega P_n^\nu(\cos\theta)(\Delta^{-1})_{n\nu,\tilde{n}\tilde{m}}[\omega R P^\mu_{\tilde{n}}(\cos\theta)\delta_{\tilde{m}\mu} + (-1)^\mu\{\Psi^o_{\tilde{n}\tilde{m}}, \sin(\mu\varphi_\gamma)\}]}{\sin^2\theta\lambda_{\tilde{n}}N_{n\nu}}. \tag{5.46}$$

The Oseen tensor for the combined motion of two domains is obtained by replacing the factor $(-1)^\mu$ by $(-1)^{\mu+1}$ in (5.45) and (5.46). If the contrast between the domain and embedding membrane surface shear viscosity vanishes equation simplifies to

$$O^{e,tot}_{\nu\mu} = \sum_n \frac{\nu\mu\omega P_n^\nu(\cos\theta)[\omega R P^\mu_n(\cos\theta)\delta_{\nu\mu} + (-1)^\mu\{\Psi^e_{n\nu}, \cos(\mu\varphi_\gamma)\}]}{\sin^2\theta\lambda_n N_{n\nu}}. \tag{5.47}$$

For the special case that the second domain sits at the south pole $\gamma = \pi$ we find $\vartheta = \pi - \vartheta_\pi$ and $\varphi = \pi - \varphi_\pi$. Therefore

$$\left.\begin{aligned}\{\cos(\mu\varphi_\pi), \Psi^e_{n\mu}\}_{\gamma=\pi,\theta} &= (-1)^\mu \omega R P^\mu_n(-\cos\theta) = (-1)^n \omega R P^\mu_n(\cos\theta),\\ \{\sin(\mu\varphi_\pi), \Psi^o_{n\mu}\}_{\gamma=\pi,\theta} &= -(-1)^\mu \omega R P^\mu_n(-\cos\theta) = -(-1)^n \omega R P^\mu_n(\cos\theta)\end{aligned}\right\} \tag{5.48}$$

and

$$\left.\begin{aligned}O^{e,tot}_{\nu\mu}[0,\theta;\pi,\theta] &= \sum_{n,\tilde{n}} \frac{(1+(-1)^{\tilde{n}-\mu})\omega^2 R\nu\mu P^\nu_n(\cos\theta)(\Delta^{-1}_\nu)_{n,\tilde{n}} P^\nu_{\tilde{n}}(\cos\theta)}{\sin^2\theta \lambda_{\tilde{n}} N_{n\nu}}\delta_{\nu\mu},\\ O^{o,tot}_{\nu\mu}[0,\theta;\pi,\theta] &= \sum_{n,\tilde{n}} \frac{(1-(-1)^{\tilde{n}-\mu})\omega^2 R\nu\mu P^\nu_n(\cos\theta)(\Delta^{-1}_\nu)_{n,\tilde{n}} P^\nu_{\tilde{n}}(\cos\theta)}{\sin^2\theta \lambda_{\tilde{n}} N_{n\nu}}\delta_{\nu\mu}\end{aligned}\right\} \tag{5.49}$$

with

$$\Delta_{\nu,\tilde{n}n} = \left\{\delta_{\tilde{n}n} - \frac{\delta\lambda_n}{\lambda_{\tilde{n}}}\frac{\pi\int_{-1}^1 \mathrm{d}x\,\mathrm{sign}(x^2-\cos^2\theta)P^\nu_{\tilde{n}}(x)P^\nu_n(x)}{N_{n\nu}}\right\}, \tag{5.50}$$

which in the case $\mathscr{H}_s = 0$ simplifies to

$$\left.\begin{aligned}O^{e,tot}_{\nu\mu}[0,\theta;\pi,\theta](\mathscr{H}_s=0) &= \sum_n \frac{(1+(-1)^{n-\mu})\omega^2 R\nu\mu P^\nu_n(\cos\theta)^2}{\sin^2\theta\lambda_n N_{n\nu}}\delta_{\nu\mu},\\ O^{o,tot}_{\nu\mu}[0,\theta;\pi,\theta](\mathscr{H}_s=0) &= \sum_n \frac{(1-(-1)^{n-\mu})\omega^2 R\nu\mu P^\nu_n(\cos\theta)^2}{\sin^2\theta\lambda_n N_{n\nu}}\delta_{\nu\mu}.\end{aligned}\right\} \tag{5.51}$$

If both domains move relative to each other but perpendicular to their connecting geodesics then the domain at the north pole will rotate around the vesicle centre with velocity $\boldsymbol{u}_\perp = (\omega_{rel,\perp}/\sqrt{2})\boldsymbol{e}_x \times \boldsymbol{r}$ such that $\check{u}^e_{\perp,\theta,1} = (\omega_{rel,\perp}/\sqrt{2})R$ and $\check{u}^e_{\perp,\theta,\nu} = 0$ for $\nu = \pm 2, \pm 3, \ldots$. Hence

$$\check{\tau}_{rel,\perp,1} = \sqrt{2}\check{\tau}_{\perp,1}[0,\theta] = \omega_{rel,\perp}(\boldsymbol{O}^{-1}_{e,tot})_{11}. \tag{5.52}$$

Similarly, for a relative motion parallel to the interconnecting geodesics the domain at the north pole will rotate around the vesicle centre with velocity $\boldsymbol{u}_\parallel = (\omega_{rel,\parallel}/\sqrt{2})\boldsymbol{e}_y \times \boldsymbol{r}$ such that $\check{u}^o_{\parallel,\theta,1} = (\omega_{rel,\parallel}/\sqrt{2})R$ and $\check{u}^o_{\parallel,\theta,\nu} = 0$ for $\nu = \pm 2, \pm 3, \ldots$. Hence

$$\check{\tau}_{rel,\parallel,1} = \sqrt{2}\check{\tau}_{\parallel,1}[0,\theta] = \omega_{rel,\parallel}(\boldsymbol{O}^{-1}_{o,tot})_{11}. \tag{5.53}$$

The diffusion coefficient perpendicular to the geodesic connecting the domains is different than along the geodesic and we find

$$\left.\begin{aligned}\frac{1}{f_\parallel} &= \eta_o R^3 \sin\theta \frac{\omega_{rel,\parallel}}{|\check{\tau}_{rel,\parallel,1}|} = \frac{\eta_o R^2 \sin\theta}{|(\boldsymbol{O}^{-1}_{o,tot})_{11}|},\\ \frac{1}{f_\perp} &= \eta_o R^3 \sin\theta \frac{\omega_{rel,\perp}}{|\check{\tau}_{rel,\perp,1}|} = \frac{\eta_o R^2 \sin\theta}{|(\boldsymbol{O}^{-1}_{e,tot})_{11}|}.\end{aligned}\right\} \tag{5.54}$$

For $\mathscr{H}_s = 0$ and $\gamma = \pi$, (5.54) simplifies, and using (5.51) we regain (4.10). In general several tasks outlined in the derivation in this section can only be performed numerically. When there is contrast in surface shear viscosities the integrals $\langle \Psi_{\tilde{n}\tilde{m}}\chi(\vartheta,\varphi)\Psi_{nm}\rangle$ must be computed. And the matrix Δ must be inverted numerically. In case of two-domain rheology and $\gamma \neq \pi$ one additionally has to numerically compute the integrals $\{\cos(\nu\varphi_\gamma), \Psi^e_{nm}\}_{\gamma,\theta}$ and $\{\sin(\nu\varphi_\gamma), \Psi^o_{nm}\}_{\gamma,\theta}$ and numerically must invert the Oseen tensor $\boldsymbol{O}_{tot}$. We will compute the effect of viscosity contrast for only

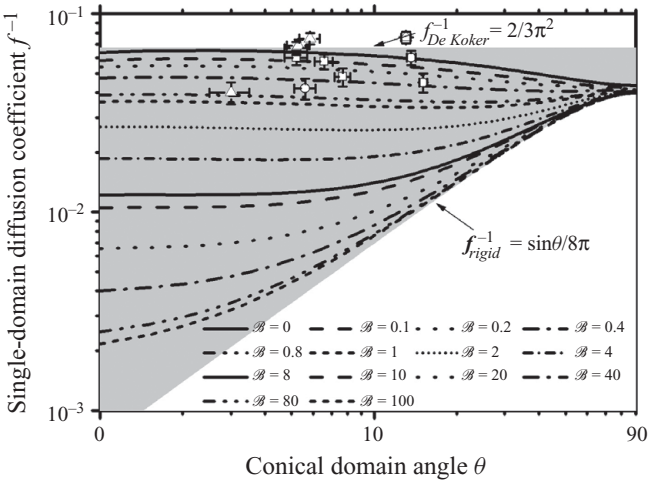

FIGURE 6. Dimensionless single-domain diffusion coefficient f^{-1} versus the conical domain angle θ for $\mathscr{H}_s = 0$ and different Boussinesq numbers $\mathscr{B} = 0$–100. The grey area extends over the region of possible single-domain diffusion coefficients where lower and upper boundary represent, respectively, the diffusion coefficient of a rigid sphere and a non viscous liquid disk in a non viscous flat membrane first derived by DeKoker equation (5.42). Experimental single-domain diffusion coefficients are incorporated in the figure for the compositions DOPC/DPPC/Chol = 16/64/20 (□), DOPC/DPPC/Chol = 40/40/20 (○), and DOPC/DPPC/Chol = 35/35/30 (△). All data falls into the regime of negligible surface shear viscosity ($\mathscr{B} < 1$).

one domain rheology. For the two-domain rheology the computation time would become quite long when considering arbitrary separations of the domains and a contrast in viscosity.

6. Single-domain rheology: results

In figure 6 we plot f^{-1}, i.e. the dimensionless single-domain diffusion coefficient versus the conical angle θ of the domain edge at different Boussinesq numbers for the case $\eta_o = \eta_i$ and $\eta_s^a = \eta_s^b$. The diffusion coefficient is very sensitive to the Boussinesq number for domains with small size. For large domains of size comparable to the radius of the vesicle, however, the variation of the diffusion coefficient with Boussinesq number is rather weak. Ultimately for large domains we rediscover (5.40) and the domain diffuses together with the entire vesicle, and the motion of the domain on the vesicle is locked to the rotation of the entire vesicle. The diffusion coefficient is bounded by the relation $2/3\pi^2 > f^{-1} > \sin\theta/8\pi$ within the grey region in figure 6 where the boundaries are given by the diffusion coefficient of De Koker (1996) corresponding to (5.42) and the rigid diffusion coefficient corresponding to (5.40). Experimental single-domain diffusion coefficients are incorporated in the figure for the compositions DOPC/DPPC/Chol = 16/64/20 (□), DOPC/DPPC/Chol = 40/40/20(○), and DOPC/DPPC/Chol = 35/35/30 (△) at a temperature of $T = 23°$C. All data falls into the regime of negligible surface shear viscosity ($\mathscr{B} < 1$).

In figure 7 we plot the single-domain diffusion coefficient versus the Boussinesq number for the case $\eta_o = \eta_i$ and $\eta_s^a = \eta_s^b$. The diffusion first decreases with the Boussinesq number but levels off when $\mathscr{B} > R/a$, where the surface is so viscous that

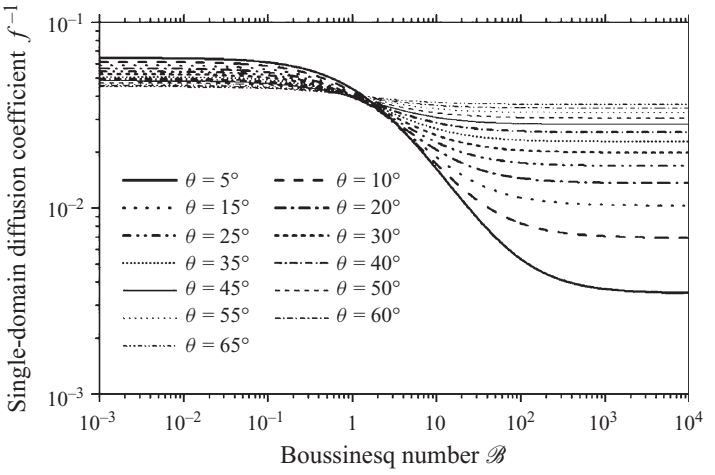

FIGURE 7. Dimensionless single-domain diffusion coefficient f^{-1} versus the Boussinesq number for $\mathscr{H}_s = 0$ and for different values of the conical domain angle θ.

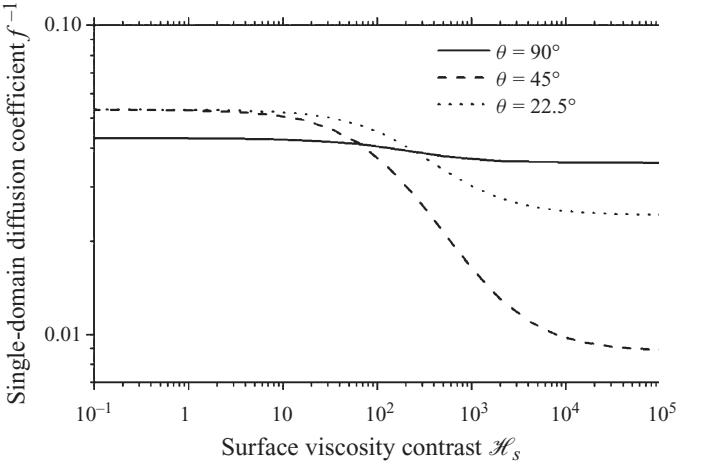

FIGURE 8. Dimensionless single-domain diffusion coefficient f^{-1} versus the surface shear viscosity contrast $\mathscr{H}_s$ for Boussinesq number $\mathscr{B} = 0.01$ (corresponding to fixed embedding membrane surface shear viscosity) and different conical domain angles θ.

it behaves like a rigid sphere with a diffusion coefficient given by (5.40) independent of the Boussinesq number. An increase of domain surface shear viscosity η_s^a at constant embedding membrane viscosity η_s^b results in higher friction and thus lowers the values of the diffusion constant. This can be seen in figure 8, where we plot the dimensionless single-domain diffusion coefficient at a fixed surface shear viscosity η_s^b of the embedding membrane against the surface shear viscosity contrast $\mathscr{H}_s$. When $\mathscr{B}\mathscr{H}_s \sin\theta \approx 1$ the diffusion coefficient decreases until it reaches a value $f^{-1}_{solid\ domain} \approx \sin\theta/8\pi$ that is lower than the diffusion coefficient of a liquid domain but higher than that of a rigid surface. The cross-over from a liquid interface to a partially rigid interface occurs when $\mathrm{Max}(\eta_s^a, \eta_s^b) \approx R\eta_o$. The change in diffusion constant is most pronounced for domains with intermediate size. Large domains diffuse mainly via rigid rotation of the vesicle already at very small surface shear

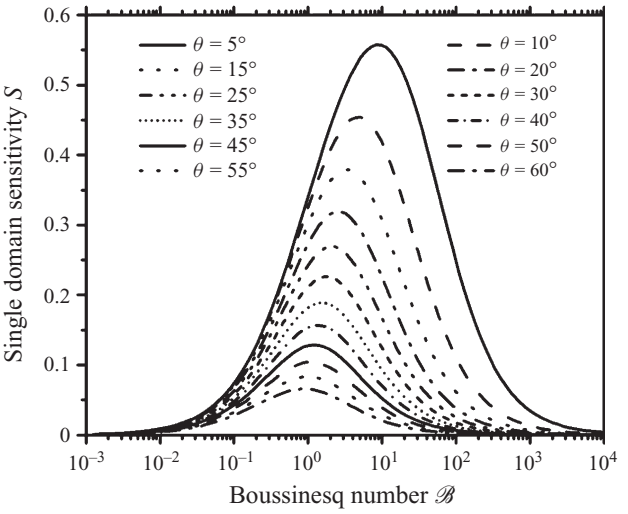

FIGURE 9. Sensitivity S of single-domain rheology versus Boussinesq number for different conical domain angles θ.

viscosity. An increase in surface shear viscosity in the domain therefore will not affect significantly the diffusion since it was already slow before the increase. For small domains, most of the vesicle remains at a low viscosity and their diffusion would not be affected by the high viscosity inside the small region of the domain. It is only for the domains of intermediate size that substantial reduction in diffusion is achieved by making the domain more viscous than the rest of the membrane. Intermediate size domains diffuse faster than a rigid vesicle at low viscosity and zero contrast. Increasing the surface shear viscosity of these domains makes a substantial fraction of the vesicle very viscous such that substantial decreasing of the diffusion occurs. Even a small domain when reaching a viscosity of $\eta_s^a \approx R\eta_o$ will start to feel the friction from the opposite site of the vesicle and will result in a decrease of diffusion coefficient substantially smaller than what is expected from a solid domain in a flat membrane. This shows that the order of the limits $\eta_s^a \to \infty$ and $R \to \infty$ may not be changed without obtaining different results. The basic result hence is that there is a cross-over from surface viscosity dominated friction towards finite size friction at roughly $\mathrm{Max}(\eta_s^a, \eta_s^b) \approx R\eta_o$. The cross-over from surface viscosity dominated friction towards finite size friction emerges in figure 9 as a peak in the sensitivity S versus $\mathscr{B}$ for the single-domain rheology. This peak is located in the regime $1 < \mathscr{B} < 1/\sin\theta$, while at low Boussinesq number ($\mathscr{B} < 1$) and at high Boussinesq number $\mathscr{B} > 1/\sin\theta$ the sensitivity is negligible. Moreover, the peak in sensitivity increases as the conical domain angle θ decreases. Since, at a fixed domain radius a and decreasing vesicle radius R the conical domain angle θ increases, we conclude that a confinement of domains to a small vesicle decreases the sensitivity and makes the measurement of the surface shear viscosity more difficult. In figure 6 the scattering of the experimental data that falls into the insensitive regime ($\mathscr{B} < 1$) is much larger than systematic variations of the surface shear viscosity with the structure of the phases.

7. Two-domain rheology: results

In § 4 we have shown that the relative diffusion of a domain measured with respect to a reference domain on the same vesicle depends on the separation between the

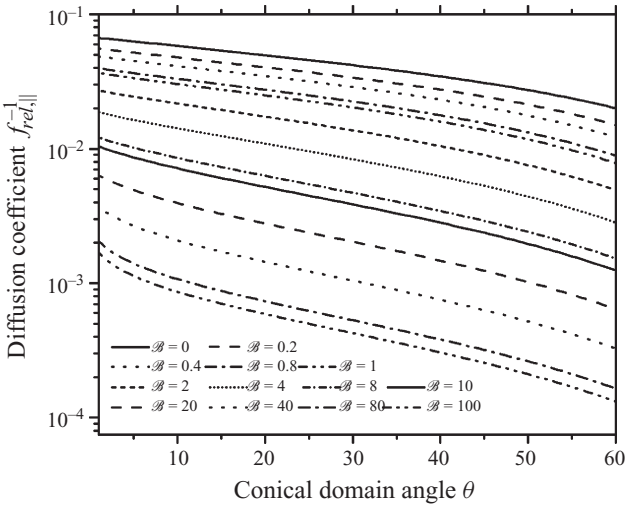

FIGURE 10. Dimensionless two-domain relative longitudinal diffusion coefficient $f_{rel,\parallel}^{-1}$ versus the conical domain angle θ for $\gamma = \pi$ and different Boussinesq numbers $\mathscr{B} = 0$–100.

domains and on the direction of the combined or relative motion. If one measures the relative motion between two domains then one must use a theory which describes the measured motion of one domain relative to the other domain. Choosing as reference domain one which is not infinitely separated from the domain of measurement has the draw back that the motions of the two domains are no longer uncorrelated. One disadvantage is that hydrodynamic interactions between the domains could give rise to a decrease of the relative diffusion of the domains as compared to the diffusion of single domains. The relative motion of both domains comes to a complete stop when both domains touch each other. To minimize the correlation between the two domains, one has to increase their separation, and the best situation will be when the two domains are located at opposite sides on the vesicle ($\gamma = \pi$), which significantly simplifies the mathematics of the relative diffusion. We therefore consider these hydrodynamic interactions for the case where one domain is located at exactly the opposite side of the vesicle than the reference domain. Figure 10 shows the relative longitudinal diffusion coefficient $f_{rel,\parallel}^{-1}$ as a function of the conical domain angle θ of the two domains for $\gamma = \pi$ and for different values of the Boussinesq number $\mathscr{B}$. Keeping the Boussinesq number fixed and changing the conical angle corresponds to decreasing the size of the vesicle at a fixed domain size and fixed rheological properties. While for a single domain the variation of the friction with the conical angle is weak, there is a pronounced dependence of the relative longitudinal domain diffusion coefficient on the conical angle. The larger the conical angle θ or the smaller the vesicle the more pronounced and the more correlated is the motion of the two domains. Relative motion of the domains becomes increasingly difficult and ultimately ceases when the vesicle is so small that both domains cover an entire hemisphere. At $\gamma = \pi$, a domain with conical angle of 30° exhibits the same relative diffusion coefficient than a small domain at a Boussinesq number that is one order of magnitude larger than that of the large domain.

Figure 11 shows the diffusion coefficient $f_{rel,\parallel}^{-1}$ as a function of the Boussinesq number $\mathscr{B}$. For $\mathscr{B} < 1$ the diffusion coefficient $f_{rel,\parallel}^{-1}$ is rather independent of the Boussinesq number and hence at $\mathscr{B} < 1$ the two-domain rheology is insusceptible to

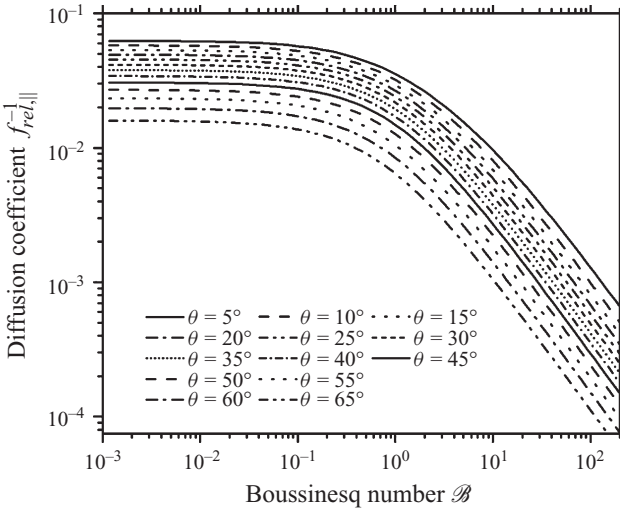

FIGURE 11. Dimensionless relative longitudinal diffusion coefficient $f_{rel,\|}^{-1}$ of two domains sitting at opposite sides of the vesicle versus the Boussinesq number for different conical domain angles θ. The diffusion coefficient shows a strong dependence on the Boussinesq number $\mathscr{B}$ for values $\mathscr{B} > 1$ making the relative longitudinal diffusion mode sensitive to $\mathscr{B}$.

the surface shear viscosity just as in the case of one domain rheology. At larger Boussinesq numbers the diffusion coefficient $f_{rel,\|}^{-1}$ of the longitudinal relative motion rapidly decreases with increasing Boussinesq number $\mathscr{B}$ and two-domain rheology becomes a sensitive rheological technique. Two-domain rheology is quite complex when considering domains separated by an arbitrary angle γ. We distinguish four modes of motion: 'combined' motion, where both domains move in the 'same direction along or perpendicular' to their interconnecting geodesic and 'relative' motion where both domains move in 'opposite directions'. It is important to note that 'relative' and 'combined' motion is a term that makes sense with respect to the interconnecting geodesic. If we consider the four modes and slowly separate the domains until they reach opposite sides of the vesicle, 'relative transversal' motion and 'combined longitudinal' motion become indistinguishable. The same is true for 'relative longitudinal' motion and 'combined transversal' motion. This can be seen in figure 12, where we plot the diffusion coefficient f^{-1} versus the domain separation γ for all four modes for a conical domain angle of $\theta = 30$ deg and for vanishing contrasts $\mathscr{K} = 0$ of the bulk and $\mathscr{K}_s = 0$ surface shear viscosities. All four modes have different diffusion coefficients. For all Boussinesq numbers $\mathscr{B}$ and all separations γ relative longitudinal diffusion has the lowest diffusion coefficient and combined longitudinal motion has the highest. The diffusion coefficient of relative motion decreases with decreasing separation angle γ. The diffusion coefficient of combined motion increases with decreasing separation angle.

Combined transversal motion and combined longitudinal motion are fairly similar at small separations. The reason for this becomes evident when considering a single domain of twice the area of the two domains. If both domains would fuse to one domain, combined transversal and combined longitudinal motion would merge to the single-domain diffusion constant of a domain with conical angle $\theta = 42.9°$. The values of those single-domain diffusion constants are shown at the left side of figure 12.

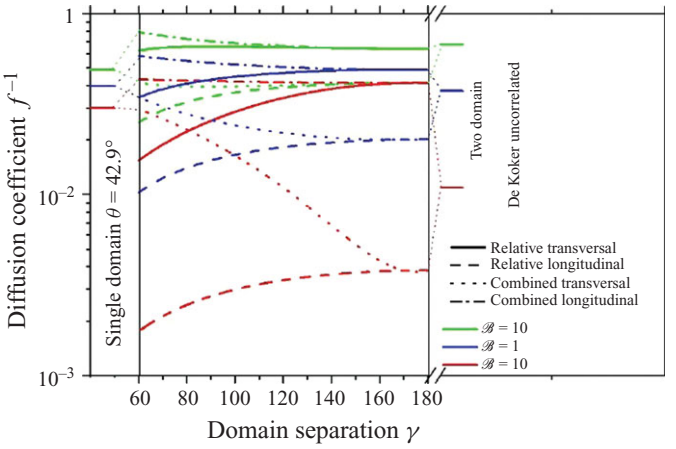

FIGURE 12. Dimensionless two-domain diffusion constants of all four modes of diffusion versus domain separation γ at three different Boussinesq numbers ($\mathscr{B} = 0, 1, 10$) and for a conical domain angle of both domains of $\theta = 30°$. To the left we show the corresponding single-domain diffusion constants of a single domain having the same area as the two domains. To the right we show the uncorrelated single-domain diffusion constant expected in a flat membrane. The splitting of the combined modes at low separation is a result of shape anisotropy. The splitting at maximum separation is a result of hydrodynamic correlations.

The splitting occurring between the combined modes at low separation is a result of the shape anisotropy of the two domains as compared to a single domain of similar area. Combined transversal and relative longitudinal motion become the same when both domains are separated by the maximal separation of $\gamma = \pi$. The mode reacting most sensitive to changes in the Boussinesq number $\mathscr{B}$ is the longitudinal relative diffusion. Combined transversal motion shows the strongest sensitivity to geometrical issues: While being rather insensitive to changes in Boussinesq number at small separations combined transversal motion becomes more and more sensitive to the Boussinesq number as the separation between both domains increases. Relative transversal motion just shows the opposite behaviour. At large separations relative transversal motion is slightly sensitive to changes in the Boussinesq number but its sensitivity become more accentuated when the domain separations become small. Both tendencies can be easily understood by considering that the transversal motions take on the character of longitudinal motions when the separation angle approaches $\gamma = \pi$. The difference in diffusion coefficients $f^{-1}_{rel,\parallel} = f^{-1}_{comb,\perp}$ and $f^{-1}_{rel,\perp} = f^{-1}_{comb,\parallel}$ at $\gamma = \pi$ shows that both domains are still correlated when being separated at maximum distance. For a comparison we show the diffusion coefficient $f^{-1}_{De\ Koker}$ corresponding to (5.42) that is expected in a flat membrane for infinite separation of the domains. The splitting of the two pairs of modes is therefore *a* measure of the hydrodynamic correlations persisting in a vesicle. The splitting between both diffusion coefficients is minimal for small domains and low Boussinesq number. The splitting increases when having larger domains or higher Boussinesq numbers. In the range $\mathscr{B} > 1/\sin\theta$, i.e. the range where single-domain rheology is insensitive to the Boussinesq number, the longitudinal relative diffusion is sensitive to the Boussinesq number. However the longitudinal relative diffusion is strongly correlated in this regime. Separation of the motion of two domains into the proper modes in a two-domain rheology is important due to the different behaviour of these modes.

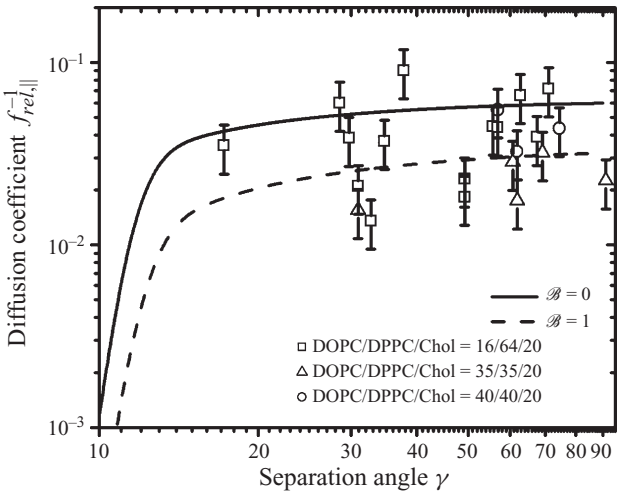

FIGURE 13. Experimental relative longitudinal diffusion coefficient of domains $f_{rel,||}^{-1}$ versus the domain separation γ for a conical domain angle of $\theta \approx 5 \pm 1$ deg for the compositions DOPC/DPPC/Chol = 16/64/20 (□), DOPC/DPPC/Chol = 40/40/20 (○), and DOPC/DPPC/Chol = 35/35/30 (△). Two theoretical curves with $\mathscr{B} = 0$ and $\mathscr{B} = 1$ are incorporated for vanishing contrast $\mathscr{H} = 0$ of the bulk and $\mathscr{H}_s = 0$ surface shear viscosities. The average experimental two-domain data suggest that the single-domain data are correct and that surface viscous effects are negligible ($\mathscr{B} < 1$).

Experimental two-domain diffusion data will usually be collected at varying separations γ. In figure 13 we depict the experimental relative longitudinal diffusion coefficient of domains $f_{rel,||}^{-1}$ versus the domain separation γ for a conical domain angle of $\theta \approx 5^\circ \pm 1^\circ$ for the compositions DOPC/DPPC/Chol = 16/64/20 (□), DOPC/DPPC/Chol = 40/40/20(○), and DOPC/DPPC/Chol = 35/35/30 (△). Two theoretical curves with $\mathscr{B} = 0$ and $\mathscr{B} = 1$ are incorporated for vanishing contrast $\mathscr{H} = 0$ of the bulk and $\mathscr{H}_s = 0$ surface shear viscosities. Although the scatter of the data is large the average experimental two-domain data suggest that the single-domain data are correct and supports the idea that $\mathscr{B} < \infty$. Surface viscous effects are negligible ($\mathscr{B} < 1$) for the mixtures and surface shear viscosities in all phases are lower than $\eta_s < 10^{-9}\,\mathrm{Ns\,m^{-1}}$. The scatter of the experimental data is more pronounced as in single-domain rheology.

In contrast to single-domain rheology, two-domain rheology, specifically the longitudinal relative diffusion becomes increasingly sensitive to the Boussinesq number at high Boussinesq numbers. One might think that this would enable measurement of high surface shear viscosities of the vesicle membrane using two-domain rheology. However, in practice a vesicle of high viscosity will have a solid rotational diffusion constant that is larger than the relative diffusion time by a factor given by the Boussinesq number $\mathscr{B}$. The two domains in the field of view of the microscope will leave the field of view of the microscope with a rate defined by the solid rotational diffusion constant. The typical change in separation of the two domains during that limited time is of the order $R\sqrt{\Delta\gamma^2} = \mathscr{B}^{-1/2}R$. Two domains of size 5 μm on opposite sides on a vesicle of typical size $R = 20\,\mu\mathrm{m}$, and surface shear viscosity $\eta_s = 10^{-6}\,\mathrm{Ns\ m^{-1}}$ will change their separation by 1 μm during the time available for the observation. Similar domains separated by less than the maximal separation will diffuse apart by less than 1 μm. Optical microscopy of resolution 1 micron

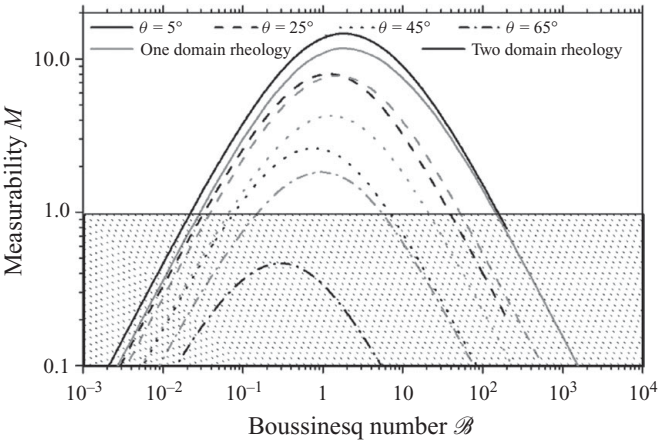

FIGURE 14. Measurability M of one domain rheology (grey) and of the relative longitudinal diffusion mode for two domains sitting at opposite sides of the vesicle (black) versus Boussinesq number $\mathscr{B}$ for different conical domain angles θ. The shaded region indicates the region non accessible by the experiments.

will therefore be useful for measurements of shear surface viscosities that are less than $\eta_s < 10^{-6}\,\mathrm{Ns\,m^{-1}}$. In single-domain rheology, one does not have these resolution requirements. A rheological technique capable of measuring the surface shear viscosity must have both high resolution and high sensitivity. In figure 14 we therefore plot the measurability M, (3.12) versus the Boussinesq number $\mathscr{B}$ for both one domain and two-domain rheology. In the plot we assume a value of $R^2/\Delta x^2_{min} = 10^3$. At similar conical domain angles θ, the measurability of one domain rheology is about a factor of 1–10 larger than for two-domain rheology. If one wishes to measure the surface shear viscosity, the one-domain rheology is superior to two-domain rheology. Two-domain rheology on the other hand has the advantage of producing a more local measurement of the surface shear viscosity, at the price of lower measurability. The variation of the measurability with the Boussinesq number $\mathscr{B}$ and the conical domain angle θ is rather similar for both techniques. Both techniques allow the measurement of surface shear viscosities in a regime $1 < \mathscr{B} < 1/\sin\theta$. Outside this regime measurements of the surface shear viscosity should not be trusted. All diffusion data aquired for the different mixtures in this paper fall into a range where only upper bounds for the surface shear viscosity can be given.

It is obvious what to expect when using multi-domain rheology. Most likely the measurability will suffer further decrease as the number of domains used for the measurement is increased. Multi-domain rheology might however give a more local measure of the surface shear viscosity and will be also mathematically more complex. Tracking the motion of more domains on a vesicle hence will not improve the problems occurring in the measurement of high surface shear viscosities. One way to overcome the low measurability at high surface shear viscosities might be to look at the coarsening kinetics of the domains. The vesicle can lower its domain line tension energy via the coalescence of domains. At high surface shear viscosities the coalescence of domains most likely will become diffusion limited. Observing the statistics of coarsening as a function of time will not require following the positions of individual domains such that the time of observation is no longer limited by the rotational relaxation time $\Delta t_{max} < D_{rot}^{-1}$. Hence the high sensitivity of

relative longitudinal diffusion together with a higher resolution achieved via long time measurements will lead to a high measurability.

8. Discussion

Diffusion of domains within cell membranes is a difficult hydrodynamic problem. Solutions to this problem must take into account the geometric constraints and the mechanical and rheological properties of the constituents. Let us discuss the effects of geometry first. We approximated the geometric shape of a vesicle by a sphere and the domain as a circular segment which adheres to the sphere. Such approximation holds if the viscous stresses at the vesicle membrane and at the domain edge are small compared to the vesicle tension and the domain edge line tension. Fluorescence microscopy images of vesicles containing ternary mixtures of lipids and cholesterol (Veatch & Keller 2003; Cicuta *et al.* 2007) show that the shapes of vesicles and domain edges can be spherical and circular, respectively. Based on this experimental evidence, we neglect fluctuations of the shapes due to finite interfacial and line tension. Our analysis of course does not apply close to the miscibility critical point, where domain shapes undergo significant fluctuations and where the line tension between the phases approaches to zero (Baumgart, Hess & Webb 2003). It also does not apply when the bending rigidities of the domains are different from the bending rigidities of the rest of the membrane such that domains bulge into the exterior liquid (Honerkamp-Smith *et al.* 2008). We have shown that the single-domain rotational diffusion experimentally observed in video microscopy of a domain on a vesicle is due to the diffusion of the domain within the vesicle if the surface shear viscosity is small $\eta_s \ll \eta R$. In vesicles of typical size of 20 μm residing in an aqueous environment ($\eta \approx 10^{-3}\,\mathrm{Ns\,m^{-2}}$) this means that only if $\eta_s \ll 2\times10^{-8}\,\mathrm{Ns\,m^{-1}}$ the domain can diffuse within the vesicle. Our upper limit for the apparent single-domain translational diffusion constant is given by De Koker's result $D_{trans} < D_{trans}^{DeKoker} = 2k_BT/3\pi^2\eta_o a$. For large surface shear viscosities $\eta_s >> 2\times10^{-8}\,\mathrm{Ns\,m^{-1}}$ the diffusion of the domain will no longer be dominated by diffusion within the membrane but by the solid rotational diffusion of the rigid vesicle as a whole. The apparent translational diffusion coefficient associated with such rigid rotational diffusion is $D_{trans}^{rigid} = k_BT/8\pi\eta_o R$. For a vesicle with radius 20 μm in water the apparent single-domain translational diffusion coefficient of a domain in a rigid vesicle is $D_{trans}^{rigid} = 10^{-2}\,\mu\mathrm{m^2\,s^{-1}}$. We have shown that the most reliable way of measuring surface shear viscosities on vesicles with domain tracking is to use single-domain rheology. In recent experiments of Cicuta *et al.* (2007) measurements of the surface shear viscosity of vesicular membranes are reported using multi-domain rheology. Cicuta *et al.* (2007) try to avoid the loss of sensitivity of single-domain rheology at high Boussinesq numbers by subtracting average diffusion to yield unbiased domain motion. No details are given how such average motion is subtracted. On a curved surface, velocities of different domains are lying in different tangent spaces to the different domains and therefore cannot be subtracted directly since such relative velocities would have components moving the domain out of the interface. Measurements of relative velocities in curved space are far from trivial. The proper way to obtain relative velocities has been outlined in (4.1)–(4.5) and corresponds to subtracting velocities of the reference domain only after parallel transport (Misner *et al.* 1973) along the geodesic connecting the reference domain to the domain of measurement. An analysis where one subtracts velocities from several reference domains, of course is a form of multi-domain rheology that cannot be interpreted correctly using single-domain rheological equations such as those of

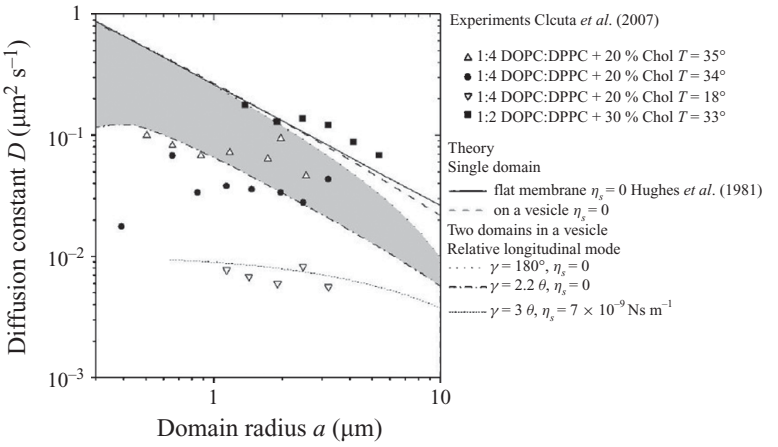

FIGURE 15. Comparison of single-domain and relative longitudinal translational diffusion with experimental data from Cicuta *et al.* (2007) for a vesicle of radius $R = 20\,\mu m$, bulk viscosity of $\eta = 10^{-3}\,Ns\,m^{-2}$, temperature $T = 300\,K$, and vanishing bulk and surface viscosity contrasts $\mathscr{H} = \mathscr{H}_s = 0$. The grey region indicates the regime where relative longitudinal diffusion can be explained by different separations γ of the domains without the need of a surface shear viscosity. Below the grey area the surface shear viscosity becomes measurable and we show a fit (short dotted line) with $\gamma = 3\theta$ and $\eta_s = 7 \times 10^{-9}\,Ns\,m^{-1}$ to the 1:4 DOPC:DPPC + 20 % cholesterol data at $T = 18°C$. Experimental data above the grey area most likely contain contributions from the other three two-domain diffusion modes. The solid and dashed line shows the theoretical predictions for a single domain in a flat membrane and on a vesicle.

Saffmann & Delbrück (1975) or such as those of Hughes *et al.* (1981). No distinction of modes has been made by Cicuta *et al.* (2007) when analysing their data. However, we might expect that subtracting average velocities will largely eliminate contributions from the three modes that contain solid rotations of the entire vesicle. One might hope that their measurements will catch the motion of the relative longitudinal mode to the neighbouring domain lying along the direction of momentary motion. Fluorescence images of the vesicles investigated by Cicuta *et al.* (2007) suggest that the density of domains is quite high such that there are always neighbouring domains in the way of motion. In figure 15 we plot the single-domain and relative longitudinal two-domain translational diffusion constants versus domain size a for a vesicle of radius $R = 20\,\mu m$ under several different geometrical situations. The single-domain translational diffusion constant $D_{Hughes} = k_B T/16\,\eta a$ for non viscous flat membrane and the single-domain translational diffusion constant on a vesicle $D_{single}^{vesicle}$ have the largest diffusion constant. The relative longitudinal two-domain translational diffusion constant in a non-viscous vesicle at maximum separation of both domains is almost a factor of two smaller than the single-domain diffusion. All experimental two-domain rheology data having properly subtracted relative motion between the two domains should lie below this line. We incorporate experimental data from Cicuta *et al.* (2007) into our graph and some of these data (the 1:2 DOPC:DPPC + 30 % cholesterol mixture at $T = 33°C$) lie above this line indicating that subtracting the motion of more than one reference domain might not properly project onto the relative longitudinal mode of two domains. Relative longitudinal diffusion depends on the separation of the two domains. In figure 15 we have plotted the largest possible value of relative longitudinal translational diffusion occurring for a separation of $\gamma = \pi$ and vanishing surface shear viscosity $\eta_s = 0$. Additionally, we plot the lowest relative longitudinal

translational diffusion constant possible for zero surface shear viscosity $\eta_s = 0$ if one discards domains that are too close $\gamma < 2.2\theta$. The grey region between this two lines hence is a region where experimentally observed diffusion constants may be explained by pure geometry without any surface shear viscosity $\eta_s = 0$. Most of the data of Cicuta *et al.* (2007) falls into this regime. The translational diffusion constants of the 1:4 DOPC:DPPC + 20 % cholesterol mixture at $T = 35°C$ can be explained equally well with $\eta_s = 0$ and $\gamma = 5\theta$ as with $\eta_s = 3 \times 10^{-9}\,\mathrm{Ns\,m^{-1}}$ and $\gamma = \pi$. Experimental data falling below the grey region cannot be explained with vanishing surface shear viscosity. Cicuta *et al.* (2007) data for the 1:4 DOPC/DPPC mixture with 20 % cholesterol at 18°C and 34°C falls below the grey region. In our measurements the slowest mode of diffusion is the longitudinal relative diffusion. We could not confirm the experimental values measured by Cicuta *et al.* (2007). In order to get a figure of merit about the surface shear viscosity their data would imply we fitted the data of Cicuta *et al.* (2007) assuming a separation between the domains of $\gamma \approx 3\theta$ that approximately corresponds to the fluorescence images presented with their data.

We found that their data for the 1:4 DOPC/DPPC mixture with 20 % cholesterol at 18°C is well fitted with the relative longitudinal mode when using a viscosity of $\eta_s = 7 \times 10^{-9}\,\mathrm{Ns\,m^{-1}}$. This viscosity is almost three orders of magnitude smaller than when fitting the same data with Saffmann & Delbrück (1975) ($\eta_s = 4 \times 10^{-6}\,\mathrm{Ns\,m^{-1}}$) showing that hydrodynamic interactions between domains cannot be neglected. Translational diffusion constants of lipids in mixtures of phospholipids and cholesterol measured with fluorescence correlation spectroscopy (Kahya & Schwille 2006) and diffusion nuclear magnetic resonance (NMR) (Filippov, Orädd & Lindblom 2004) report values of $0.1 \times 10^{-8}\,\mathrm{cm^2\,s^{-1}} < D_{lipid} < 20 \times 10^{-8}\,\mathrm{cm^2\,s^{-1}}$. If we assume that those lipids diffuse as individuals without forming larger complexes, neglect the non-continuous structure of the membrane on the molecular scale, we may fit those single-lipid translational diffusion constants using Saffmann & Delbrück (1975). We assume a hydrodynamic membrane radius of the lipid is of the order of 5 Å. Under these circumstances the lipid diffusion constants correspond to surface viscosities of $3 \times 10^{-8}\,\mathrm{Ns\,m^{-1}} > \eta_s > 1 \times 10^{-10}\,\mathrm{Ns\,m^{-1}}$, which is consistent with our experimental data and with our interpretation of the domain diffusion but inconsistent with using Saffmann & Delbrück (1975) for the domain diffusion and inconsistent with the experimental data of Cicuta *et al.* (2007). If the lipids do not diffuse as individuals but in the form of larger complexes, the surface shear viscosity extracted from the lipid diffusion data will be somewhat lower than when assuming individual diffusion. Moreover our value of the surface shear viscosity corresponds to a Boussinesq number slightly smaller than unity $\mathscr{B} \approx 1$, which is just below the regime of good measurability of the technique. The lever rule states that properties like the surface shear viscosity of the coexisting phases should not vary with the area fraction each phase occupies. The data of Cicuta *et al.* (2007) varies with the area fraction and violates the lever rule. In our measurements surface shear viscosities are negligible and there is no violation of the lever rule.

Our experimental data, our analysis of the data and our interpretation of the experiments therefore differ from Cicuta *et al.* (2007). Diffusion constants of the slowest mode are larger than diffusion constants of Cicuta *et al.* (2007). Most of the reduction in diffusion constant on the vesicle is an effect of a decreasing separation γ of the domains. The diffusion is mainly affected by the hydrodynamic interactions mediated primarily via the bulk fluid, and surface shear viscosity of the membranous phases are at least three orders of magnitude smaller than anticipated by Cicuta *et al.* (2007).

So far, we have neglected the contrast in surface shear viscosity in our discussion. In the limit of vanishing surface shear viscosity the diffusion constant of a liquid domain is larger by a factor of $32/3\pi^2 = 1.08$ than that of a solid domain. Deviations of the result of De Koker (1996) from the results of Hughes *et al.* (1981) are limited to 15 % over the entire range of surface shear viscosities. The curvature of the vesicle does not change these effects if one discards the domains of intermediate size. Hence the approximation to use the same surface shear viscosity for the domain and the majority phase of the membrane for vesicular phases of small surface shear viscosity is believed to lead to errors not exceeding 15 %. Given the uncertainties in conditions in the experimental data these deviations from (3.9) appear to be of minor impact to the numerical values extracted from the data. The theory derived here is for one and two domains diffusing in a homogeneous membrane. In experiments there usually are several domains on a vesicle. We might consider the suspension of domains in the vesicle as an effective medium with an effective surface shear viscosity. However, once one of the surface shear viscosities results in a viscous length scale of the order of the typical geometric extensions of the system, the diffusing domain will sense and react in its diffusion to all geometrical details within that range. Our measurements (not shown) indicate that the presence of other domains suppresses relative transversal diffusion in a way, such that relative transversal diffusion becomes comparably slow to relative longitudinal diffusion. This in turn might be used to detect length scales of the S_0 phase domains in the three phase coexistence region S_0, L_α, L_0. Great care needs to be taken if one wants to extract rheological properties of one of the constituents of such a system.

9. Conclusions

Single-domain rheology and two-domain rheology on a vesicle are two ways to measure the surface shear viscosity of membranes in a vesicle. The ratio of surface to bulk viscosities defines a viscous length scale. Only when the viscous length scale falls between the size of the domain and the size of the vesicles, can a surface shear viscosity be measured easily. To achieve a high measurability of the surface shear viscosity the diffusion must be sensitive to the surface viscosity and must be resolved. We demonstrate that the best domain-tracking method to resolve the surface shear viscosity is the single-domain rheology. Different modes of diffusion in two- or multi-domain rheology have different sensitivity and resolution. A domain rheology measurement should decompose the motion of the domains into normal modes of diffusion. The decomposition is important because hydrodynamic interactions between domains confined to the same vesicle reduce the relative longitudinal diffusion constant stronger than the other modes of diffusion. This makes the relative longitudinal mode more sensitive to the surface shear viscosity than other modes of diffusion. The gain in sensitivity is achieved by a loss of resolution and does not increase the range where surface shear viscosities can be measured. Our experiments on vesicle do not confirm the diffusion constants measured in experiments of Cicuta *et al.* (2007). Our interpretation suggests that the observed reduction in diffusion constants is mainly due to hydrodynamic interactions mediated by the water and only a minor contribution is due to the viscous membrane. Our experimental diffusion constants correspond to surface shear viscosities that differ by at least three orders of magnitude from those extracted by Cicuta *et al.* (2007). The diffusion of domains in vesicles depends on all geometrical details in the surrounding of the domain that are within the range of the viscous length scale. Thus our work will help and inspire experiments on the diffusion of domains on spherical surfaces.

We thank H. Brand for useful discussion, W. Reichstein and J. Köhler for help with the vesicle preparation. P. T. was supported by the program 'Juan de la Cierva' (JCI-2009-04192). P. D. and T. M. F. acknowledge support by the National Science Foundation under CHE-0649427. T. M. F. and Z. K. acknowledge support by the German Science Foundation under Fi548/10-1/11-1 and the Jordanian Higher Council for Science and Technology.

REFERENCES

Angelova, M. I., Soléau, S., Méléard, Ph., Faucon, J. F. & Bothorel, P. 1992 Preparation of giant vesicles by external AC electric-fields – kinetics and applications. *Program. Colloid Polym. Sci.* **89**, 127–131.

Bagatolli, L. A. & Gratton, E. 2000 Two photon fluorescence microscopy of coexisting lipid domains in giant unilamellar vesicles of binary phospholipid mixtures. *Biophys. J.* **78**, 290–305.

Baumgart, T., Hess, S. T. & Webb, W. W. 2003 Imaging coexisting fluid domains in biomembrane models coupling curvature and line tension. *Nature* **425**, 821–824.

Beattie, M. E., Veatch, S. L., Stottrup, B. L. & Keller, S. L. 2005 Sterol structure determines miscibility versus melting transitions in lipid vesicles. *Biophys. J.* **89**, 1760–1768.

Berne, B. J. & Precora, R. 2000 *Dynamic Light Scattering with Applications to Chemistry, Biology and Physics*. Dover.

Brown, D. A. & London, E. 1998 Functions of lipid rafts in biological membranes. *Annu. Rev. Cell Devel. Biol.* **14**, 111–136.

Cicuta, P., Keller, S. L. & Veatch, S. L. 2007 Diffusion of liquid domains in lipid bilayer membranes. *J. Phys. Chem.* B **111**, 3328–3331.

Daniels, D. R. & Turner, M. S. 2002 Diffusion on membrane tubes: a highly discriminatory test of the Saffman–Delbrück theory. *Langmuir* **23**, 6667–6670.

Danov, K., Dimova, R. & Pouligny, B. 2000 Viscous drag of a solid sphere straddling a spherical or flat surface. *Phys. Fluids* **12**, 2711–2722.

De Koker, R. 1996 Domain structures and hydrodynamics in lipid monolayers. PhD dissertation, Stanford University.

Dimova, R., Dietrich, C., Hadjiisky, A., Danov, K. & Pouligny, B. 1999*a* Falling ball viscosimetry of giant vesicle membranes: finite-size effects. *Eur. Phys. J.* B **12**, 589–598.

Dimova, R., Dietrich, C. & Pouligny, B. 1999*b* Motion of particles attached to giant vesicles: falling ball viscosimetry and elasticity measurements on lipid membranes. In *Giant Vesicles* (ed. P. Walde & P. Luisi), chap. 15, p. 221. John Willey & Sons.

Edwards, D. A., Brenner, H. & Wasan, D. T. 1991 Interfacial transport and rheology. *Butterworth–Heinemann Ser. Chem. Engng Boston*, pp. 104–111.

Engelman, D. M. 2005 Membranes are more mosaic than fluid. *Nature* **438**, 578–580.

Fischer, Th. M. 2003 The drag on needles moving in a Langmuir monolayer. *J. Fluid Mech.* **498**, 123–137.

Fischer, T. M., Dhar, P. & Heinig, P. 2006 The viscous drag of spheres and filaments moving in membranes or monolayers. *J. Fluid. Mech.* **558**, 451–475.

Fischer, T. M. & Lösche, M. 2004 Pattern formation in Langmuir monolayers due to long range electrostatic interactions. In *Lecture Notes in Physics, Molecules in Interaction with Surfaces and Interfaces* (ed. R. Haberlandt, D. Michel, A. Pöppl & R. Stannarius), vol. 634, pp. 383–394. Springer.

Filippov, A., Orädd, G. & Lindblom, G. 2004 Lipid lateral diffusion in ordered and disordered phases in raft mixtures. *Biophys. J.* **86**, 891–896.

Gaus, K., Gratton, E., Kable, E. P. W., Jones, A. S., Gelissen, I., Kritharides, L. & Jessup, W. 2003 Visualizing lipid structure and raft domains in living cells with two-photon microscopy. *Proc. Nat. Acad. Sci.* **100**, 15554–15559.

Heinig, P., Wurlitzer, S., John, t. & Fischer, Th. M. 2002 Stability criterion for three phase intersection points in monolayers. *J. Phys. Chem.* B **106**, 11951–11960.

Honerkamp-Smith, A. R., Cicuta, P., Collins, M. D., Veatch, S. L., den Nijs, M., Schick, M. & Keller, S. L. 2008 Line tensions, correlation lengths and critical exponents in lipid membranes near critical points. *Biophys. J.* **95**, 236–246.

Hughes, B. D., Pailthorpe, B. A. & White, L. R. 1981 The translational and rotational drag on a cylinder moving in a membrane. *J. Fluid Mech.* **110**, 349–372.

Kahya, N. & Schwille, P. 2006 How phospholipid-cholesterol interactions modulate lipid lateral diffusion, as revealed by fluorescence correlation spectroscopy. *J. Fluoresc.* **16**, 671–678.

Khattari, Z., Heinig, P., Wurlitzer, S., Steffen, P., Lösche, M. & Fischer, Th. M. 2002 Wetting in asymmetric quasi-2d-systems. *Langmuir* **18**, 2273–2279.

Klingler, J. F. & McConnell, H. 1993 Brownian-motion and fluid-mechanis of lipid monolayer domains. *J. Phys. Chem.* **97**, 6096–6100.

Korlach, J., Schwille, P., Webb, W. W. & Feigenson, G. W. 1999 Characterization of lipid bilayer phases by confocal microscopy and fluorescence correlation spectroscopy. *Proc. Nat. Acad. Sci.* **96**, 8461–8466.

Kubo, R. 1957 Statistical-mechanical theory of irreversible processes 1. General theory and simple applications to magnetic and conduction problems. *J. Phys. Soc. Japan* **12**, 570–586.

Levine, A. J. & MacKintosh, F. C. 2002 Dynamics of viscoelastic membranes. *Phys. Rev.* E **66**, 061606.

Misner, C. W., Thorne, K. P. & Wheeler, J. A. 1973 *Gravitation.* W. H. Freeman and Company.

Mukherjee, S. & Maxfield, F. R. 2000 Role of membrane organization and membrane domains in endocytic lipid trafficking. *Traffic* **1**, 203–211.

Naji, A., Levine, A. J. & Pincus, P. A. 2007 Corrections to the Saffman–Delbrück mobility for membrane bound proteins. *Biophys. J.* **93**, L49–L51.

Peters, R. & Cherry, R. J. 1982 Lateral and rotational diffusion of bacteriorhodopsin in lipid bilayers: experimental test of Saffman–Delbrck equations. *Proc. Nat. Acad. Sci. USA* **79**, 4317–4321.

Petrov, E. P. & Schwille, P. 2008 Translational diffusion in lipid membranes beyond the Saffman–Delbrück approximation. *Biophys. J.* **94**, L41–L43.

Prasad, V., Koehler, S. A. & Weeks, E. R. 2006 Two-particle microrheology of quasi-2D viscous systems. *Phys. Rev. Lett.* **97**, 176001–176004.

Radhakrishnan, H. A. & McConnell, H. M. 1999 Cholesterol-phospholipid complexes in membranes. *J. Am. Chem. Soc.* **121**, 486–487.

Reichl, L. E. 1980 *A Modern Course in Statistical Physics.* Edward Arnold, pp. 545–595.

Riess, J. G. 2002 Fluorous micro- and nanophases with a biomedical perspective. *Tetrahedron* **58**, 4113–4131.

Russel, W. B., Saville, D. A. & Schowalter, W. R. 1989 Colloidal dispersions. In *Cambridge Monographs on Mechanics and Applied Mathematics* (ed. G. K. Batchelor), pp. 31–35. Cambridge University Press.

Saffman, P. G. & Delbrück, M. 1975 Brownian-motion in biological-membranes. *Proc. Nat. Acad. Sci. (USA)* **72**, 3111–3113.

Sickert, M., Rondelez, F. & Stone, H. A. 2007 Single-particle Brownian dynamics for characterizing the rheology of fluid Langmuir monolayers. *Eur. Phys. Lett.* **79**, 66005–66010.

Simons, K. & Ikonen, E. 1997 Functional rafts in cell membranes. *Science* **387**, 569–572.

Singer, S. J. & Nicholson, G. L. 1972 The fluid mosaic model of the structure of cell membranes. *Science* **175**, 720–731.

Trabelsi, S., Zhang, S., Lee, T. R. & Schwartz, D. K. 2006 Linactants: surfactant analogues in two dimensions. *Phys. Rev. Lett* **18**, 037802.

Veatch, S. L., Gawrisch, K. & Keller, S. L. 2006 Closed-loop miscibility gap and quantitative tie-lines in ternary membranes containing diphytanoyl PC. *Biophys. J.* **90**, 4428–4436.

Veatch, S. L. & Keller, S. L. 2002 Organization in lipid membranes containing cholesterol. *Phys. Rev. Lett.* **89**, 268101–268104.

Veatch, S. L. & Keller, S. L. 2003 Separation of liquid phases in giant vesicles of ternary mixtures of phospholipids and cholesterol. *Biophys. J.* **85**, 3074–3083.